NASA CR-120948
ADL 73235

NASA

PRODUCTION OF FIBERS BY A FLOATING ZONE FIBER DRAWING TECHNIQUE

(NASA-CR-120948) PRODUCTION OF FIBERS BY A FLOATING ZONE FIBER DRAWING TECHNIQUE Final Report J.S. Haggerty (Little (Arthur D.), Inc.) May 1972 65 p CSCL 11D

N72-29532

Unclas
G3/15 38599

J. S. HAGGERTY

ARTHUR D. LITTLE, INC.

prepared for

NATIONAL AERONAUTICS AND SPACE ADMINISTRATION

NASA LEWIS RESEARCH CENTER
CONTRACT NAS 3-14328
L. WESTFALL, PROJECT MANAGER

NASA CR-120948
ADL 73235

FINAL REPORT

PRODUCTION OF FIBERS BY A FLOATING ZONE FIBER DRAWING TECHNIQUE

by

J. S. Haggerty

prepared for

NATIONAL AERONAUTICS AND SPACE ADMINISTRATION

May 1972

CONTRACT NAS 3-14328

NASA Lewis Research Center
Cleveland, Ohio 44135
L. Westfall, Project Manager

Arthur D Little, Inc.

TABLE OF CONTENTS

LIST OF FIGURES

LIST OF FIGURES (Cont)

LIST OF TABLES

I. SUMMARY

A CO_2 laser heated, floating zone fiber growth process was developed during this program. The resulting Al_2O_3 fibers exhibited the highest room temperature strengths ever reported for large diameter fibers as well as the highest specific creep rupture strengths observed at 1093°C and 1316°C (2000°F and 2400°F). Single crystal fibers of TiC and Y_2O_3 were grown for the first time.

An optical system was developed to focus four CO_2 laser beams onto the surface of a feed rod permitting the formation of highly controllable molten zones. The optical system permitted energy densities and angle of incidence of the beams to be adjusted over wide ranges. This optical system was incorporated into the controlled atmosphere, fiber growth furnace developed under NAS 3-13479.

The two principal advantages of a CO_2 laser heat source are that ambient atmospheres may be freely selected to optimize fiber properties and the laser has no inherent temperature limit, so extremely high melting point materials can be melted. Both advantages were demonstrated during this program. Heavily Cr-doped Al_2O_3 fibers were grown in highly oxidizing atmospheres which is not possible with known crucible contained melt processes. TiC fibers were grown from melts for which no crucible material or incandescent heat source exists due to its high melting point (≈3200°C, 5800°F).

Chromium-doped Al_2O_3 fibers exhibited room temperature flexural strengths up to $9.64 \times 10^9 N/m^2$ (1.4×10^6 psi) uncoated, in the as-grown condition, in a humid atmosphere. To our knowledge, this is the highest strength ever observed with large diameter fibers. Average room temperature tensile strengths of later Cr-doped Al_2O_3 fibers ranged from approximately 3.4×10^9 to 4.1×10^9 N/m^2 (500,000 to 600,000 psi). These strengths are substantially higher than observed with other Al_2O_3 fibers. Average tensile strength of 0.027 cm (0.011 inch) diameter fibers at 1093 and 1316°C (2000 and 2400°F) were 11.1×10^8 and 7.5×10^8 N/m^2 (162,000 and 109,000 psi), respectively. These are also higher than observed with other Al_2O_3 fibers. One hundred-hour creep rupture lives of the Cr-doped Al_2O_3 fibers were approximately 1.460×10^6 and 1.27×10^6 cm (575×10^3 and 500×10^3 inches) at 1093 and 1316°C (2000 and 2400°F), respectively. This represents approximately four to five fold improvement over the best published results at 1093°C (2000°F). We found no basis for comparison at the higher temperature, however, the relatively small drop exhibited in long time strengths is extremely encouraging.

The room temperature and elevated temperature strengths of the TiC fibers are encouraging even though they were not as high as achieved with Al_2O_3 fibers. Testing was limited to only a few samples, but room temperature strengths up to $1.54 \times 10^9 N/m^2$ (224,000 psi) and a 1093°C (2000°F) strength of $0.5 \times 10^9 N/m^2$ (73,000 psi) were observed. It is believed that the strengths can be improved substantially with higher quality feed rods as well as the use of dopants. It should be noted that the rule of mixture properties

based on these results would make TiC reinforced metal matrix composites higher in performance than existing superalloys.

The Y_2O_3 fibers were free of internal and surface defects. They appeared highly susceptible to a water vapor stress corrosion mechanism which probably resulted in the observed low strengths. The material was abandoned as a candidate for fiber reinforcement of metal matrices because of its low elastic modulus [(1.03 to $1.10 \times 10^{11} N/m^2$)(15 to 16×10^6 psi)].

The fiber properties achieved in this program represent significant advances in the state-of-the-art and make the potential properties of fiber reinforcement metal matrix composites extremely promising. All program objectives were met on schedule at the proposed level of funding.

II. INTRODUCTION

Arthur D. Little, Inc., proposed and developed under the sponsorship of NASA Lewis a floating zone process for growing fibers of very high melting point materials. The principal advantage of this type of process is the melt does not contact any material except the feed rod and growing fiber with which it is inherently in chemical equilibrium. Thus, contamination of the melt from a crucible is eliminated as a factor and materials can be produced in fiber form for which no crucible material exists. Under NASA Contract NAS 3-13479 the technical feasibility and advantages of the process were demonstrated.[1]

Incandescent heaters were used principally throughout much of the first program even though it was known that this type of heat source imposed many of the atmosphere restrictions and temperature limitations typical of crucible-contained melts. Experiments with a small 10 watt CO_2 laser demonstrated the advantages of this type of heat source for the floating zone process. Ambient atmospheres can be freely selected, and the laser has no upper characteristic temperature limit. The exploratory program summarized in this report used a CO_2 laser heat source exclusively to grow fibers of materials which had not been previously available as well as in ambient atmospheres which cannot be used with high temperature crucibles.

All of the program's objectives were met on schedule. The strengths of Cr-doped Al_2O_3 (ruby) fibers grown under this program substantially exceeded the program's high temperature strength goal [(6.9×10^8 N/m^2 at 1093°C) (100,000 psi at 2000°F)], and they probably represent the highest strengths ever achieved with large diameter fibers. The specific creep-rupture properties of these fibers represent at least a four-fold improvement over any previously published results. Substantially improved metal matrix composites should be possible based on the properties of these fibers.

This report summarizes the equipment, the growth conditions and the feed materials used to produce single crystal fibers of doped and undoped Al_2O_3, Y_2O_3 and TiC.

III. FIBER GROWTH AND EVALUATION PROGRAM

A. GROWTH APPARATUS

1. CO_2 Laser Heat Source

Under the terms of this contract, Arthur D. Little, Inc., supplied at its expense, a CO_2 laser capable of forming controlled melts of materials like Y_2O_3, Al_2O_3, TiC and TiB_2. A thermal analysis indicated that, for the most demanding case, the total heat losses from a 0.15 cm (0.060 inch) diameter TiB_2 feed rod would be approximately 200 watts. Thus, a suitable laser must have had a CW output in excess of 200 watts.

After evaluating the CO_2 lasers which were commercially available in January 1971, with maximum output powers in excess of 250 watts, a Photon Sources Model 300 was purchased. The laser was delivered in mid-March 1971 and has been operated for approximately 700 hours carrying out this as well as other experimental programs. This comment is made simply to convey our feeling that gas lasers are sufficiently reliable and economical to be used as production tools.

As in any crystal growth process, the heat source for the fiber growth process must be controllable and stable. Our specifications called for adjustable CW output power from 30 to 375 watts which were to be stable after 30 minutes warm-up to within +/- 3% per hour and +/- 1.5% per 10 seconds. Continuous CW operation is preferred for crystal growth, since higher-than-average peak power densities in a pulsed mode accentuate evaporization losses. The laser has been successfully operated at power levels from 8 to 450 watts. Short-term power stability (to 10^{-6} sec) is good; long-term stability was not as good as hoped. The only serious discrepancy between performance and specifications was that the laser emits a beam whose polarization is spatially and time variant. This caused difficulty with, and ultimately the redesign of, the beam splitting optics described in the next section.

2. Laser Optics

The optical system consists of three functional components: a) the beam expanding and pointing optics, b) the beam splitter and c) the beam splitting and focusing optical bench.

The beam expanding and pointing optics are drawn schematically in Figure 1 and photographed in Figure 2. The CO_2 laser beam path has been drawn onto the photograph with arrowheads pointing in the direction of propagation. The beam is expanded by means of a lens (a) and a 25.4 cm (10 inch) focal length spherical mirror (b). Twelve and seven-tenths cm (5 inches) and 5.85 cm (2 1/2 inch) focal length lenses are used to expand the 1 cm (1/2 inch) beam by two to four times, respectively. Parallel rays are reflected from the spherical mirror when the lens is positioned at a distance from the mirror (d).

$$d = 25.4 \text{ cm (10 inches)} + \text{lens focal length}$$

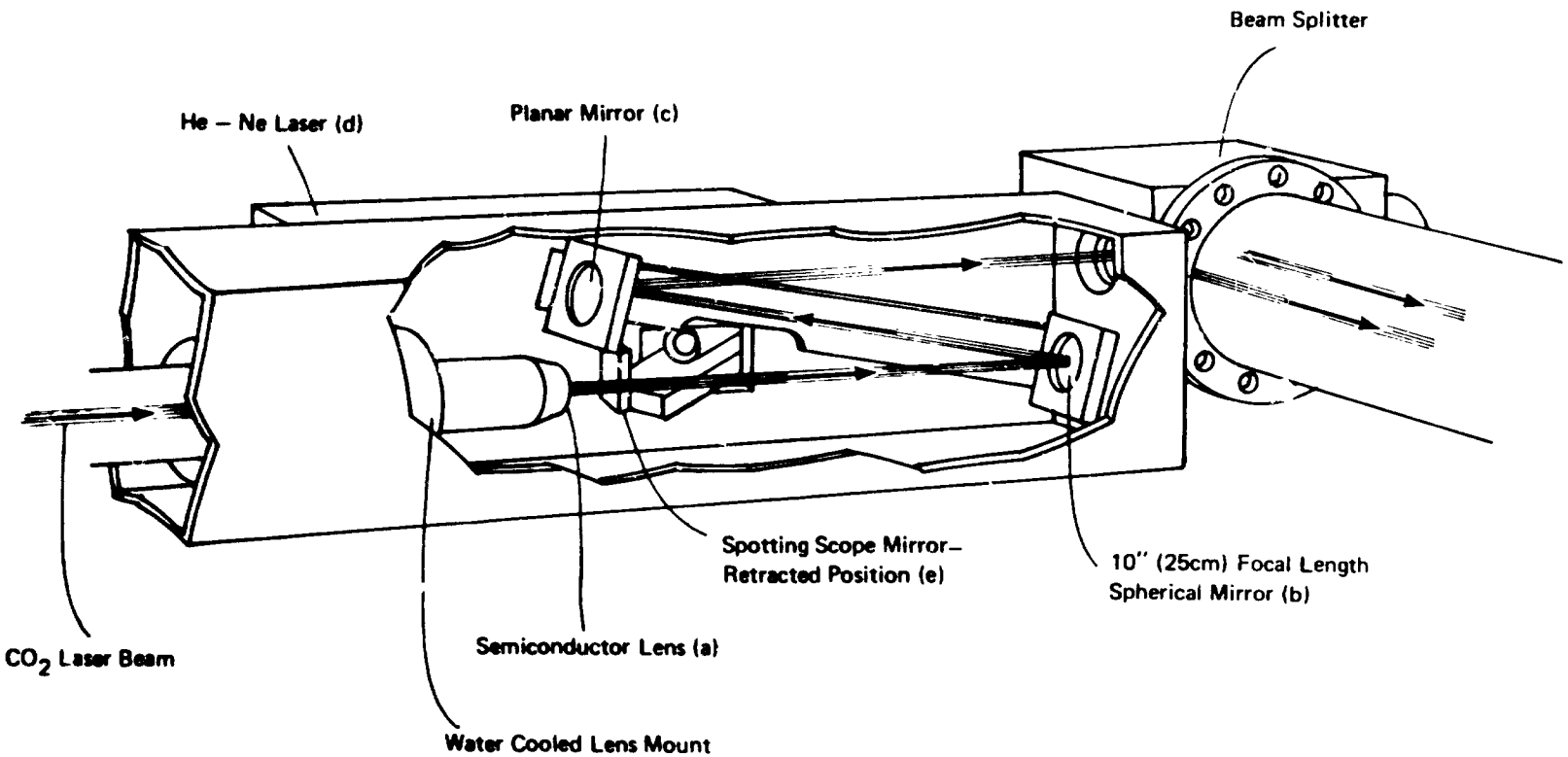

FIGURE 1 BEAM EXPANDING AND POINTING OPTICS

FIGURE 2 BEAM EXPANDING AND POINTING OPTICS WITH BEAM SPLITTER

Wher the distance is larger, the beam converges; and when it is shorter, it diverges. In principle, positioning the lens can be used to vary the energy density on the molten zone by effectively acting as a zoom. We have found that commercial quality GaAs and Ge lenses contain excessive wedge to permit the zoom feature to be used for lens excursions in excess of 2.54 cm (1 inch) The angular deflection of the beam due to wedge is proportional to (n-1), where n is the refractive index of the lens. The effect of non-uniform lens thickness is thus much greater with semiconductor optical materials ($n \simeq 4$) than with conventional optical materials ($n \simeq 1.5$). The beam passes from spherical mirror (b) to the planar mirror (c) where it is reflected parallel to the original laser beam and expanded by a factor determined by the focal length of the lens and its position relative to the spherical mirror. The vertical displacement (height) of the beam is adjustable. Mirrors (b) and (c) are attached to a plate which pivots about the center of mirror (b). A rotation about this point effects the height but not the angle of the transmitted beam.

A He-Ne laser (d) is used to position the feed rod and seed at the correct location in the furnace. The He-Ne laser beam (visible as red) follows the same path as the CO_2 laser beam with the exception that the beam splitter acts as a front surface mirror and only one beam enters the furnace. Mirrors (e) and (f) as well as a microscope lens (not visible in Figure 2) rotate on a common support. In the position shown in Figure 2, the virtual focal point of the microscope objective lens coincides with the focal point of the 25.4 cm (10-inch) focal length spherical mirror (b); thus, when properly aligned, the He-Ne beam will follow the same path as the CO_2 laser beam. During fiber growth, the two mirrors are rotated out of the path of the CO_2 laser beam. The back of mirror (e) is shielded with a sandblasted aluminum strip to diffuse the CO_2 laser beam if it should be turned on with the mirror assembly in its path.

The beam splitter consists of a watercooled, coated GaAs window (g) and a front surface mirror (h). The coating thicknesses on the window surfaces are designed to reflect 50% of the beam from the front surface of the window (g) and to have no reflection losses from the rear surface. Half of the incident beam is transmitted to mirror (h) where it is reflected parallel the the portion of the beam reflected from the front surface of the GaAs window. The window and the mirror are coupled on a common support which is positioned by 2 micrometers. The micrometers provide up-down and left-right displacement of the two exiting beams. Thus, combined with the up-down displacement provided with the beam expander, the positions and directions of the beams leaving the beam expander can be independently adjusted.

The two beams from the beam splitter travel to the furnace through a tube which terminates at a window flange (Figure 3). The two NaCl windows mounted in the flange assembly are transparent to visible and IR wavelength light. The entire optical path is hermetically sealed to insure the safety of operating personnel and to provide a dry atmosphere for the salt windows.

FIGURE 3 PHOTOGRAPH SHOWING CONNECTION OF OPTICS TO FURNACE

After entering the furnace through the two salt windows, the laser beams enter the beam splitting and focusing assembly photographed in Figure 4. The beam paths have been drawn on the photograph, and arrowheads indicate the direction of propagation. Each of the two entering beams follows a path which is the mirror image of the other. The beams are intercepted first by semicircular mirrors (a) and (b) which reflect half of the incident beams to spherical mirrors (c) and (d). The other halves are intercepted by plane mirrors (e) and (f) which reflect the beams to spherical mirrors (g) and (h). The micrometer drives are adjusted to focus the beams reflected from the four 15.2 cm (6 inch) focal length mirrors (c), (d), (g) and (h) on a common spot (i) corresponding to the position of the molten zone.

The beam size and aspect ratio (width/height) at the point in space corresponding to the molten zone (i) are adjusted by varying the position of the four spherical mirrors and their angle relative to the plane defined by the two incident beams. The minimum spot size is achieved by positioning the four spherical mirrors so the distances from the surface of the molten zone to the front surface of each mirror is exactly 15.2 cm (6 inches). The incident energy density can be reduced by positioning the spherical mirrors at distances which are either greater than or shorter than their focal lengths. The spot size can also be adjusted by varying the position of the lens relative to the spherical mirror in the beam expanding and pointing assembly. The heights of the spots are reduced relative to their widths by the astigmatism resulting from tilting the four spherical mirrors. This also varies the angle of incidence of the beams on the zone. Thus, the energy density, the aspect ratio of the impinging beams and their angle of incidence can be varied with the optical system. The aspect ratio and the angle of incidence are not completely independent of one another; however, considerable adjustment is possible by varying the convergence or divergence of the beam emitted from the beam expander.

Figure 5 shows a photograph of an Al_2O_3 fiber being grown with the optical system described above.

The only major modification to the optical system from its original configuration has been in the beam splitter (g and h in Figure 2). The original beam splitter was a 5.1 cm (2 inch) diameter Ge single crystal designed to reflect 50% of an unpolarized laser beam.

The performance of dielectric coatings is strongly dependent on the angle of incidence and polarization of the incident beam. The reflected and transmitted portions of the beam from this beam splitter varied in total power and energy distribution due to the previously noted problem with spatially and time variant polarization of the emitted CO_2 laser beam. The effect of beam polarization is minimized with a normal angle of incidence. Thus, the geometry was modified to provide a near normal angle of incidence on a GaAs single crystal beam splitter. The Ge beam splitter was damaged when the water cooling was temporarily interrupted. This modification resulted in two nearly identical beams entering the beam splitting and focusing optical bench.

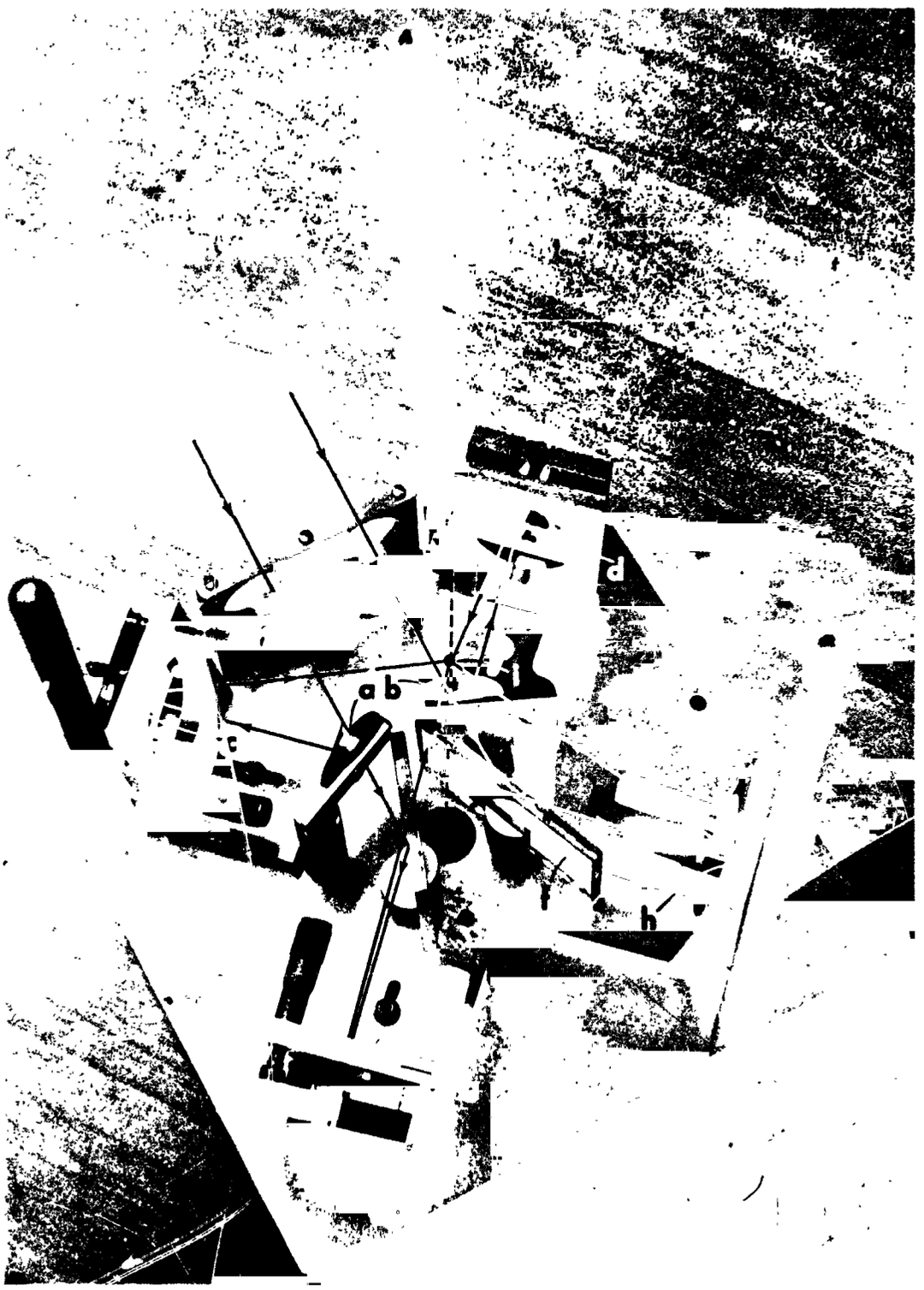

FIGURE 4 BEAM SPLITTING AND FOCUSING OPTICAL BENCH

FIGURE 5 PHOTOGRAPH OF Al_2O_3 FIBER BEING GROWN WITH CO_2 LASER HEAT SOURCE

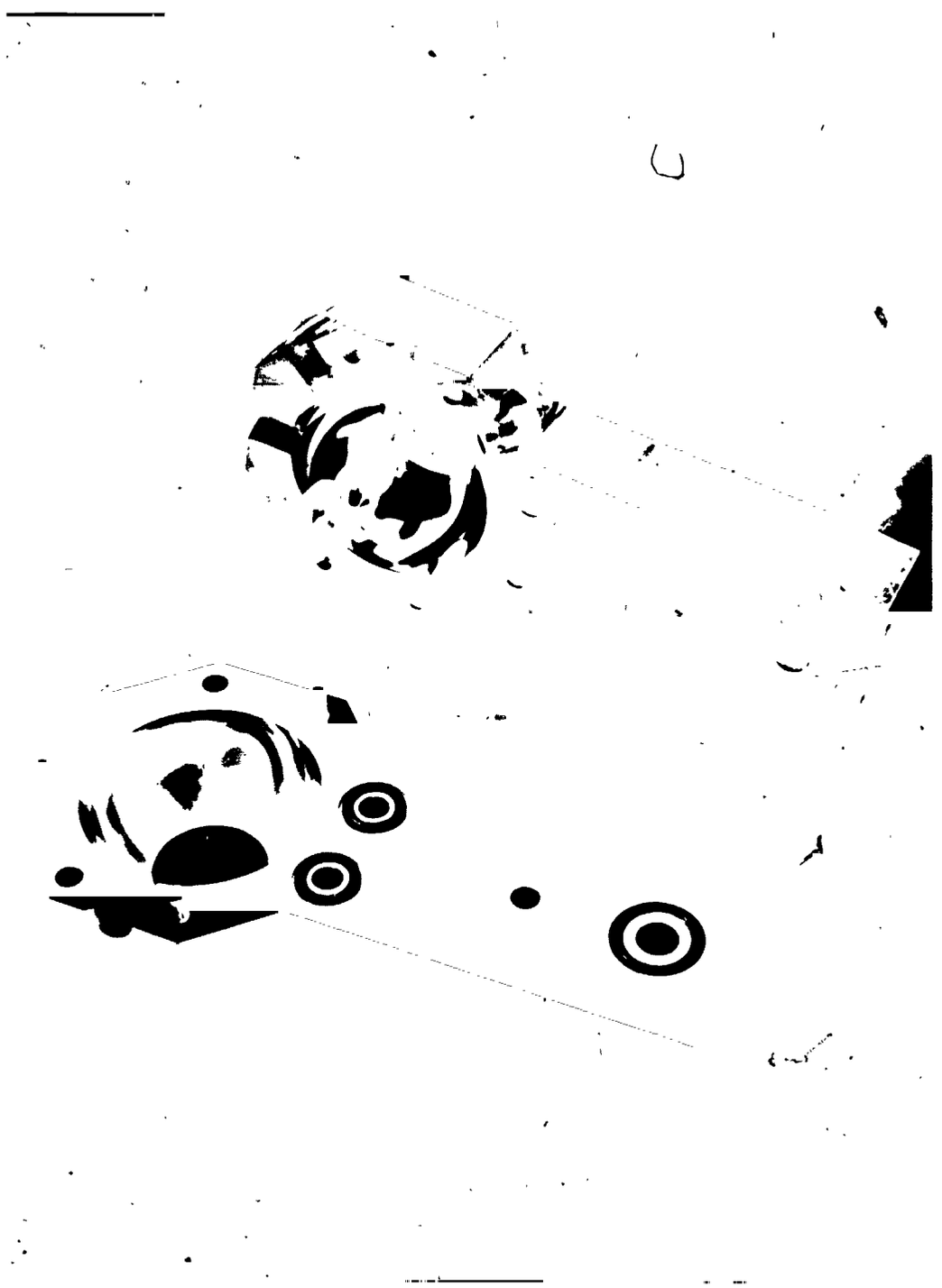

FIGURE 6 SPHERICAL RADIATION SHIELD DISASSEMBLED

FIGURE 7 SPHERICAL RADIATION SHIELD POSITIONED IN FIBER GROWTH FURNACE

3. Spherical Radiation Shield

A spherical radiation shield was designed and constructed to refocus emitted radiation and reflected 10.6μm radiation back onto the area of the molten zone. This shield proved necessary for TiC, since the absorption coefficient for 10.6μm radiation appears to be approximately 0.3 rather than 0.7 to 0.8 as reported.(2) The power level required to melt 0.11-cm (0.040 inch) diameter TiC rods without the shield approached the maximum capacity of the laser (~450 watts) compared with 145 watts calculated on the basis of reported absorptivities.

The completed spherical radiation shield is shown disassembled in Figure 6 and positioned in the furnace in Figure 7.

The shield is copper, cooled with water. The inner surfaces of the sphere are plated with a hard, bright gold to permit cleaning without degradation of the surface finish. The water cooling is introduced by a single co-axial tubing which acts as the support for the spherical radiation shield. This feature permits positional adjustments to be made easily. The sphere parts along the horizontal equator and the lower half is removable for cleaning purposes. Alignment is not disturbed during cleaning since the upper, supported half always remained in place. Registry of the two hemispheres is maintained by the two dowel pins shown in Figure 6. The water coolant is divided and flows along two parallel tubulations in the upper half of the shield. It then enters the lower half of the shield at the two "O"-ring seals adjacent to the sphere and exits at the co-axial tube through a conventional connector shown in Figure 7.

The spherical radiation shield is extremely effective in controlling radiant heat losses. The power required to grow a ruby fiber from a 0.15-cm (0.060 inch) diameter fiber feed rod is approximately 50 watts compared with 90 watts required for an unshielded molten zone. Similarly, the power level required to grow Y_2O_3 fibers was reduced from 125 watts to 70 watts. The sphere's effectiveness with the carbides was spectacular. TiC feed rods (0.15 cm (0.060 inch) in diameter) were melted with 125 to 150 watts whereas 470 watts was required to maintain a molten zone with unshielded 0.11-cm (0.040 inch) feed rods. This resulted from refocusing reflected 10.6μm radiation.

4. Fiber Growth Furnace

The controlled atmosphere fiber growth furnace, consisting of the chamber, supporting structure as well as feed-rod-insertion and fiber-withdrawal assemblies remains essentially unchanged from the apparatus constructed under NAS 3-13479. The assembled apparatus is shown (with resistance heated power supply) in Figure 8.

The furnace chamber is a rectangular parallel-piped approximately 60 cm (2 feet) high, 30 cm (1 foot) deep and 30 cm (1 foot) wide. Window and access ports were positioned to give maximum flexibility and visibility

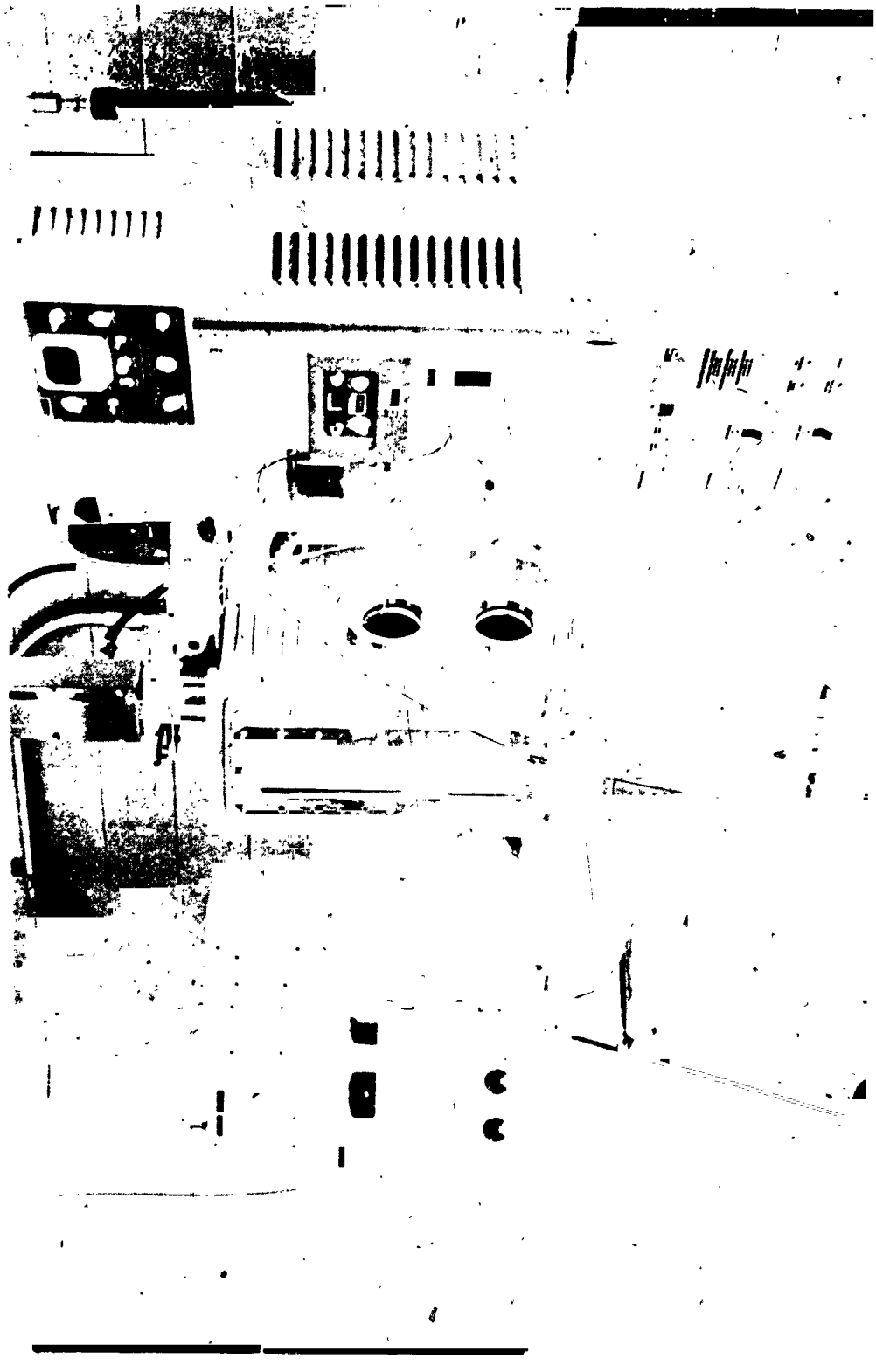

FIGURE 8 PHOTOGRAPH OF FIBER GROWTH APPARATUS IN RESISTANCE HEATED CONFIGURATION

During vacuum and $1x10^5 N/m^2$ (15 psig) operation, stress levels will not exceed $1.4x10^6 N/m^2$ (20,000 psi) in the 0.635 cm (1/4 inch) thick water-cooled stainless steel walls (water cooling not needed with laser heat source) and $6.9x10^6 N/m^2$ (1000 psi) in the 1.59 cm (5/8 inch) thick tempered Pyrex glass window. These stress levels provide adequate margins for safety. The furnace chamber, pulling-head assembly is supported on rubber shock mounts to minimize vibration transmitted from the support structure.

The gear boxes and drive motors for the pulling head were previously connected to the furnace by flexible drive cables. The flexible shafts used to couple the gear boxes to the pulling heads were replaced during this contract. It was found that they were rigid enough to transmit vibration from the floor to the shock mounted furnace as well as introducing some vibration of their own due to apparent binding and lack of torsional stiffness. The gear boxes are now coupled by shafts with universal joints on either end to insure uniform rotational speed. The shafts are keyed to permit free axial expansion and contraction while maintaining torsional rigidity. The right angle turn in power transmission is made with 90° helical-gear boxes which are virtually free of back lash. This modification has improved the isolation and smoothness of the fiber growth furnace.

Fiber withdrawal and feed-rod insertion mechanisms are ADL-MP furnace pulling heads. Unlike the standard MP Crystal Growing Furnace, the rates of travel in these pulling heads can be independently controlled. This feature permits the attenuation ratio, and thus, the fiber diameter to be continuously adjusted during a growth run. This feature was used to produce the necked test samples described in a following section.

The pulling heads are mounted in x-y positioners to permit precise alignment of the growth axis with the focal point of the laser beams. The x-y positioners are based on commercial units manufactured by the Stoelting Company, Chicago, Illinois. It was claimed that dovetails were designed to support both tensile and compressive loading so that the same units were used without modification on upper and lower pulling heads. It was found that the units had considerable drag when loaded in tension and did not always follow the micrometer drive under spring-loading.

The atmospheric seal in the x-y positioner assembly is provided by a bellows; O-rings form the seal between the bellows and the chamber walls, between the pulling head and the bellows, and between the shaft and the gland assembly.

The positioning of the furnace relative to the CO_2 laser and related optics are shown in Figure 2 and 3. The position of the beam-splitting and focusing optical bench in the furnace chamber are shown in Figure 7. The chamber required no modification for use with the CO_2 laser heat source, since it was originally designed to maximize flexibility in selection of heat sources. Based on our experience with this furnace system, a production unit would be substantially simpler in construction details.

B. Mechanical Testing Apparatus

1. Creep Rupture

Two four-station, controlled atmosphere creep-rupture apparatus were constructed to test the long-time strengths of fibers.

The individual furnaces were made by winding 0.051 cm (0.020 inch) diameter Pt-10% Rh wire on 0.95 cm (3/8 inch) internal diameter by 7.6 cm (3-inch) long mullite tubes. The externally wound tubes were cast into 3.8 cm (1 1/2 inch) outside diameter castable Al_2O_3. Additional insulation was provided by two layers of 0.38 cm (1/8 inch) thick Fiberfrax (Carborundum Co.) felt. Temperatures up to 1361°C (2400°F) were achieved with approximately 200 watts of power (current≈10 amps, voltage≈20V). The uniform temperature hot-zone in these furnaces is approximately 1.9 cm (3/4 inch) long.

Furnaces are supported simply with adjustable tubing clamps which also hold the Fiberfrax insulation in place. The axes of the furnaces were adjusted to coincide with the center lines of the fiber grips with the entire furnace adjusted plumb.

Microswitches, positioned directly under the loading weights, were used to stop the clocks at the time of failure.

The individual fiber, grip loading-weight and furnace configurations are shown schematically in Figure 9. Torque-free, tensile loadings were insured by spherodizing the ends of the fibers. The interface between the as-grown fiber and the remelted sphere was reliable stress levels up to $48.4 \times 10^7 N/m^2$ (70,000psi). Beyond that stress level, a large fraction of the fibers failed at one of the two spherodized ends upon, or soon after, loading. Necked gauge-length samples were used for high stress level testing. The 8.25 cm (3 1/4 inch) diameter by 10.15 cm (4 inch) long aluminum cans hold up to 4.55-5.45kg (10 to 12 pounds) of lead shot.

A flowing argon atmosphere was used in all creep rupture tests until test times exceeded 3000 hours at which point tests continued in an air atmosphere.

The only serious deficiency of these testing furnaces was that the entire chamber had remained closed while any of the fibers were still intact. This resulted in only partial use of the test apparatus after one or more fibers failed or in suspected premature failures of fibers which were cooled and unloaded while unused test stations were reloaded. This is discussed more thoroughly later; however, in the future, the furnace stations will be isolated from one another to avoid this problem.

2. High Temperature Tensile Testing Apparatus

All high temperature strength tests were carried out in tension under an argon atmosphere in the apparatus shown schematically in Figure 10. The furnace was the same as those used in the creep-rupture apparatus. The concentric, clear plastic tubes provided a simple, but effective, sliding seal.

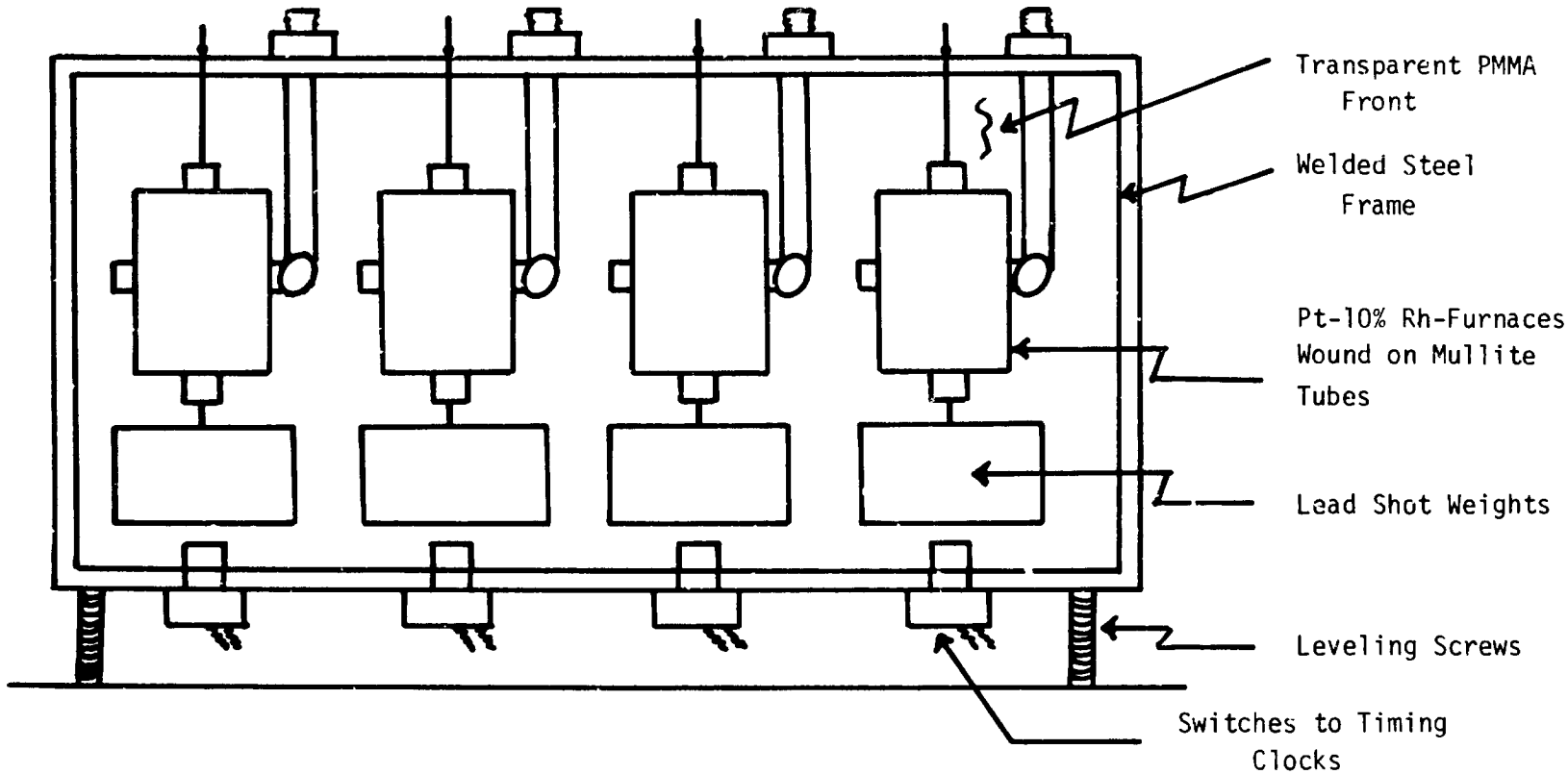

FIGURE 9 SCHEMATIC REPRESENTATION OF CREEP-RUPTURE TEST APPARATUS

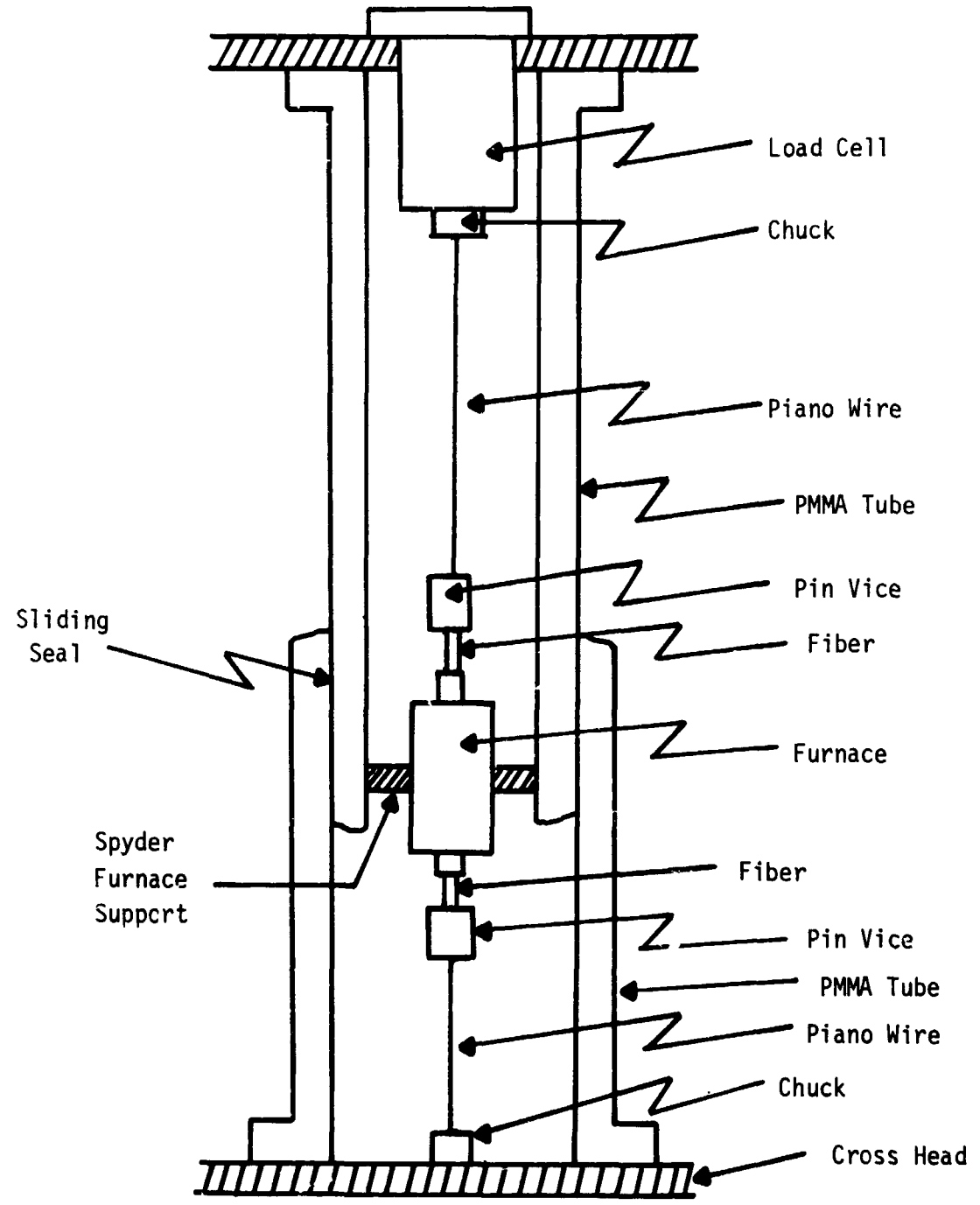

FIGURE 10 SCHEMATIC REPRESENTATION OF HIGH TEMPERATURE TENSILE TEST APPARATUS

Tests were carried out in the following manner. After installing the sample, the chamber was flushed with argon. Back diffusion of air was prevented by passing the exit gas through a glycerin bubbler. The furnace was then heated to the test temperature [(either 1093 or 1316°C)(2000 or 2400°F)] over a period of 15 to 30 minutes. The sample was loaded at a crosshead rate of 0.5 cm (0.2 inch)per minute once the test temperature was reached.

Gripping these high-strength, high-temperature test samples proved extremely difficult. Many combinations of epoxies, solders and hypodermic tubing were used with limited success. Degradation of the fiber surfaces and/or unintentionally induced bending moments caused many fibers to break in the vicinity of the grips. Also, uniform diameter fibers often broke just out of the hot-zone of the furnaces at stress levels near 48.4 to 55.2x10^{7}N/m^2 (70,000 to 80,000 psi).

All of these problems were resolved with the test sample configuration shown in Figure 11. Gripping proved straightforward and virtually all of the samples broke in their gauge lengths. The only exceptions broke in the region of the necks and were not included in the reported data. With the expanded cross sections, the samples could be gripped with pin vices. Gripping was improved by dipping the large diameter portions of the fibers in a diluted air drying glue and then rolling them in 80 mesh SiC. This provided sufficient mechanical interference that slippage was never encountered.

This samples geometry also circumvented the problem of unrepresentative failures of the uniform diameter fibers. Sapphire has been reported to exhibit a minimum in tensile strength at approximately 400 to 600°C (930 to 980°F) by several authors.(3,4,5) Thus, with test temperatures of 1093 to 1316°C (2000 to 2400°F), the samples were weaker outside of the hot zone and failed at the point of minimum strength [(approximately 48.4x10^{7}N/m^2)(70,000 psi)]. With this necked sample configuration, the tensile stress level was reduced by a factor of 3.3 to 6.5 outside of the gauge lengths which coincided with the hot zones of the furnace.

Producing necked test samples which are representative of the actual growth conditions is a unique capability of the floating zone fiber growth process. Attenuation ratios were simply varied during growth to produce the desired fiber diameter. All other investigators have used chemical or hot gas polishing techniques to reduce the cross sections of the gauge lengths; thus, their samples are not truly representative of the as-grown material.

C. Feed Rods

Feed rods of Al_2O_3 (doped and undoped), Y_2O_3, TiC, TiB_2 and unstabilized ZrO_2 were ordered for this program.

The Al_2O_3 rods represented typically marketed grades for all commercial sources. They were:

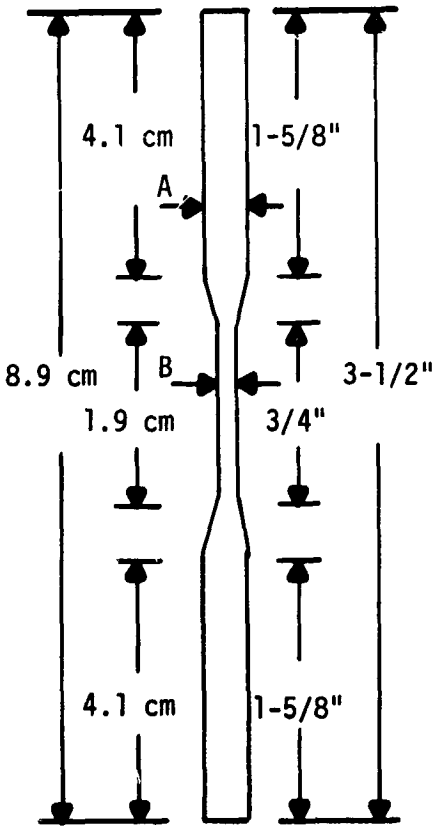

	Case 1	Case 2
A =	0.034" (0.086 cm) or	0.028" (0.071 cm)
B =	0.020" (0.051 cm) or	0.011" (0.028 cm)

FIGURE 11 SAMPLE GEOMETRY USED FOR HIGH TEMPERATURE CREEP-RUPTURE AND TENSILE TESTING

Degussa AL-23
Coors 995 pink
McDanel AP 35
McDanel AV 30
Linde Ruby

The chemical analysis supplied with these samples are given in Table I. Emission spectrographic analysis of the feed rods and selected fibers (except for McDanel AV 30) are given in Table II. These emission spectrographic analyses were made by Jarrel-Ash Division/Fisher Scientific Co.

Feed rods of the other materials were ordered on a fixed price basis from the Haselden Co. Feed rods 0.152 cm (0.060 inch) in diameter by 6.35 cm (2 1/2 inches long were to be machined from hot pressed billets. Our specifications called for purities to be in excess of 99.99% and density to be in excess of 90% with an overall maximum axial variation to be less than +/- 1%. After many delays, the TiC rods, a TiB_2 billet and a Y_2O_3 billet were delivered. Haselden was apparently unable to fabricate a sound, unstabilized ZrO_2 billet. Feed rods of TiB_2 and Y_2O_3 were machined from the Haselden billets at a local ceramic grinding house. Selected samples of these feed rods were characterized with respect to density (apparent and pycnometric), porosity and phase identification analyses by microstructural analyses; phase and lattice parameter determinations by X-ray diffraction analyses, and impurity analysis by X-ray fluorescence and emission spectrographic analyses. All of the analyses were carried out at ADL with the exception of the emission spectrographic analyses which were made by Kent Laboratories. The results of these analyses are summarized in Table III.

Our analyses showed that the Al_2O_3 feed rods generally conformed to the vendor's specifications. The absence of sodium in our analyses is anomalous, but the issue was not worth the expense of resolving. As discussed later, and as agreed in our Work Plan, Al_2O_3 growth conditions were not to be optimized in this program.

As indicated in Table III, characterization of the TiC, TiB_2 and Y_2O_3 feed rods received considerably more emphasis. Based on physical parameters (density, porosity, etc.), all three materials appeared satisfactory and all data was self-consistent.

The differences between the apparent densities and the pycnometric densities are entirely consistent with the surface roughness of the samples, since micrometer measurements give peak-to-peak diameters. If the differences between apparent and bulk densities are assigned entirely to errors in diameter measurements, then

$$\Delta d = \frac{1}{2} d \frac{\Delta \rho}{\rho}$$

where

d = diameter

ρ = density

TABLE I

SUMMARY OF FEED ROD CHEMICAL ANALYSES SUPPLIED BY VENDORS

(percentage by weight)

Impurity	McDanel AP-35	McDanel AV-30	Coors 995 (pink)	Linde Ruby	Degussa AL-23
Cr_2O_3			.22	5.8	
SiO_2	.7	3.0	.16	.13	.1
Fe_2O_3	.07	.1	.05	.29	.05
MnO				.013	
MgO	.07	1.1	.23	.05	.2
SnO_2				.057	
CaO	.03	.22	.05		.05
Na_2O	.05	.06	.05		.2
B_2O_3			.07		

TABLE II

EMISSION SPECTROGRAPHIC ANALYSES OF Al_2O_3 FEED RODS AND FIBERS

	COORS 995-PINK			DEGUSSA AL-23			LINDE RUBY			McDANEL AP-35			
Element	0.060" Feed Rod	Fiber SS Melt	Initial Clear Zone	0.039" Feed Rod	Fiber SS Melt	Initial Clear Zone	0.060" Feed Rod	Fiber SS Melt	Initial Clear Zone	0.060" Feed Rod	Fiber SS Melt	Fiber SS Melt	Initial Clear Zone
B	VFT	VVFT		VVFT	VVFT		VVFT	VVFT		VVFT	VVFT	VVFT	VVFT
Mg	L	L		L	L-M	L	VVFT VFT	VVFT VFT	FT	T-L	T-L	L	T-L
Al	H	H		H	H	H	H	H	H	H	H	H	H
Si	L	T-L		T	T	FT	VFT	VVFT-VFT	VVFT VFT	L-M	L	L-M	L-M
Ca	VFT	VFT		VFT	VFT	VFT				VFT	VFT	VFT	
Ti	FT	VFT-FT		VFT	VFT	VFT	VFT		VFT	FT	FT	VFT-FT	
V	VFT	VVFT-FT		VVFT VFT	VVFT VFT							VVFT-VFT	
Cr	L-M	L-M		FT	VFT	VVFT	M	M	L-M	FT-T	L-M	VFT-FT	VFT FT
Mn	VFT FT	VFT		VFT	VVFT	VVFT	FT			VFT	VFT	VVFT	VVFT
Fe	T-L	T		FT-T	VFT-FT	VFT	VFT	VVFT	VVFT	T	FT	FT-T	VFT-FT
Ni	VFT FT	VFT		VFT	VVFT		VVFT	VVFT		VFT		VVFT	VVFT
Cu	VVFT-VFT	VFT		VVFT-VFT	VVFT-VFT	VVFT	VVFT-VFT	VVFT-VFT	VVFT	VVFT-VFT	VVFT-VFT	VVFT-VFT	VFT
Ag					VVFT	VVFT		VVFT	VVFT	VVFT		VVFT	VVFT
Ba										FT	FT	FT	
Pb							VVFT						

KEY:

ND - Not Detected T .01 -.1%

VVFT <.0001% L .1 - 1%

VFT .0001% - .001% M 1% - 10%

FT .001% - .01% H >10%

TABLE III

CHARACTERISTICS OF HASELDEN SUPPLIED MATERIALS

Material	Apparent Density (gm/cm^3)	Bulk Density (gm/cm^3)	Reported Density (gm/cm^3)	Apparent Bulk Porosity (%)	Measured Porosity (%)	Lattice Parameter (Å)	Reported Lattice Parameter (Å)	Phases	Impurities with Concentrations in Excess of 0.001%
TiC (end)	4.559	4.67	4.85-4.93	0*	0.2	4.3249	a = 4.300 to 4.327	TiC, SiO_2	NA
TiC (mid)		4.66		0*	0.25	4.3257		TiC, SiO_2**	Si,Cr,Fe
TiB_2 (end)	4.317	4.47	4.52	1.5	0.9	a=3.0286 c=3.2294	a = 3.028 c = 3.228	TiB_2, SiO_2	NA
TiB_2 (mid)		4.43			0.9	a=3.0290 c=3.2275		TiB_2, SiO_2**	Si,Cr,Fe
Y_2O_3 (end)	4.705	4.86	4.84	0	0	10.6080	a = 10.601	Y_2O_3	NA
Y_2O_3 (mid)		4.88			0	10.6037		Y_2O_3	Ti,Si, B

NA Not available

* A theoretical x-ray density of 4.6733 gm/cm^3 was calculated for the measured lattice parameter (4.3249A) which corresponds to a composition of $TiC_{.725}$.

** The apparent concentration of SiO_2 in the middle samples was approximately 1/3 to 1/2 the level in the end samples.

Thus, for TiC the surface roughness would only have to be 1.83×10^{-3}cm (.00072 inch) to account for the difference between the apparent and pycnometric densities. The agreement of densities of the samples taken from the end and central regions of the billets indicate surprisingly axial density uniformity.

Chemical and phase identification analyses indicated serious deficiencies in the materials received from Haselden, particularly the TiC and TiB_2. The end regions of these samples contained high concentrations of Si, Cr and Fe. Quantitative X-ray diffraction analyses revealed up to 10 weight percent of α quartz (SiO_2) in the end sections of the TiC and TiB_2 rods. The levels of SiO_2 in the mid-sections of the TiC and TiB_2 rods were 1/2 to 1/3 the levels observed in the ends. These results are qualitatively consistent with microstructural analysis. Second phases were observed in TiC and TiB_2 samples in the range of 0.5 to 3% by volume. Quantitatively, there are some inconsistencies between pycnometric densities, observed porosities, volume fractions of second phases and chemical analysis. However, it was clear that the samples were so contaminated that they were useful only for the purpose of learning the specific problems each of the materials presented in growing fibers.

Microstructural analyses indicate that the TiC and Y_2O_3 samples were uniform in density down to the scale of individual grains. The TiB_2 samples contained large randomly distributed pores. Their size corresponded approximately to the larger of the two grain sizes in the hot pressed rods. It was suspected that they were large enough to interrupt or otherwise perturb the fiber growth process.

D. Growth Conditions

The CO_2 laser-heated floating zone fiber growth process intrinsically permits free selection of many normally-fixed process variables. These include ambient atmosphere, direction of growth (up or down), crystallographic growth direction, attenuation ratio which effects the melt-surface-area to melt-volume ratio, growth rate, energy density, angle of beams relative to molten zone, radiation shielding, multiple pulling, etc. In addition to these variables, feed rod characteristics, such as dopants, impurities, density, stoichiometry, must also be considered as process variables. During this program, all of these process variables have been adjusted over wide ranges with effects on resultant fiber properties; however, we did not attempt and do not claim to have defined optimized growth conditions with this formidable matrix of process variables. In general, once conditions were defined which produced controlled, reproducible fibers with signficant properties, they remained fixed for production of sample batches. Below we have listed the range of conditions under which fibers of each material have been grown.

1. Ambient Atmospheres

Al_2O_3 -

Air - pressures from 6.65 to $1.03 \times 10^5 N/m^2$ (50 μm Hg to 0 psig)

Ar - pressures from 6.65 to $1.17 \times 10^5 N/m^2$ (50 μm Hg to 2 psig)

95% Ar - 5% H_2 - pressures from 6.65 to $1.17 \times 10^5 N/m^2$ (50 μm Hg to 2 psig)

33% Ar - 66% O_2 - pressures from 4.32×10^4 to $1.17 \times 10^5 N/m^2$ (-20" Hg to 2 psig)

Y_2O_3 -

Ar - pressure equal to $2.92 \times 10^5 N/m^2$ (5 psig)

33% Ar - 66% O_2 - pressure equal to $1.03 \times 10^5 N/m^2$ (0 psig)

50% Ar - 50% O_2 - pressure equal to $8.65 \times 10^4 N/m^2$ (-10" Hg)

Ar + water vapor - pressure at $1.03 \times 10^5 N/m^2$ (0 psig)

TiC -

95% Ar - 5% H_2 - pressure equal to $1.10 \times 10^5 N/m^2$ (1 psig)

95% Ar - 5% CH_3 - pressure equal to $1.10 \times 10^5 N/m^2$ (1 psig)

Ar - pressures from 1.10×10^5 to $1.17 \times 10^5 N/m^2$ (1 to 2 psig)

2. Direction of Growth

Al_2O_3 - up and down

Y_2O_3 - up and down

TiC - up and down

3. Crystallographic Growth Axis

Al_2O_3 - unseeded showed no preferred growth axis

seeded to a and c axis growth direction

Y_2O_3 - unseeded showed no preferred growth axis

seeded to a pole 14° from <100> growth axis

TiC - unseeded generally grew within 15° of a <110> growth axis

seeded to a <111> growth axis

4. Growth Rates

Al_2O_3 - 5.9 to 290 cm/hr (114 in/hr)

Y_2O_3 - 5.5 to 29 cm/hr(2.17 to 11.4 in/hr)

TiC - 2.95 to 29 cm/hr (1.21 to 11.9 in/hr)

5. Energy Density and Beam Angle

Energy densities not characterized, individual spot sizes approximately equaled feed rod diameter.

Beam angle of incidence varied from +/- 10° relative to horizontal.

6. Radiation Shielding

None

1.9 cm (3/4 inch) diameter cylindrical Ta shield

3.8 cm (1 1/2 inch) diameter spherical shield

7. Number of Times Melted

Al_2O_3 - single and double pulls

Y_2O_3 - single and double pulls

TiC - single, double and triple pulls

E. FIBER EVALUATION

1. Testing Procedures

a. Room Temperature

Room temperature strengths have been evaluated 4-point bending, buckling and tensile tests. Four-point bending tests were used initially as a screening test, but as fiber strengths increased beyond 6.9×10^8 N/m^2 (100,000 psi), this test was abandoned. The buckling test was used for all subsequent screening tests.

In the standard ASTM 4-point bending test (Test C-75-64), the total fiber length is 8 fiber diameters and the test span is 6 fiber diameters long. Compliance with those specifications for an 0.051 cm (0.020 inch) diameter fiber would give test sample lengths of the order of 0.40 cm (0.160 inch) and only 0.1 cm (0.040 inch) of the fiber subjected to the maximum bending stress. These dimensions are clearly too small to give representative

FIGURE 12 Al_2O_3 FIBER BENT TO A RADIUS OF CURVATURE LESS THAN 2.5 CM (1 INCH) CORRESPONDING TO A STRESS IN EXCESS OF 2.68×10^9 N/m^2 (390,000 PSI)

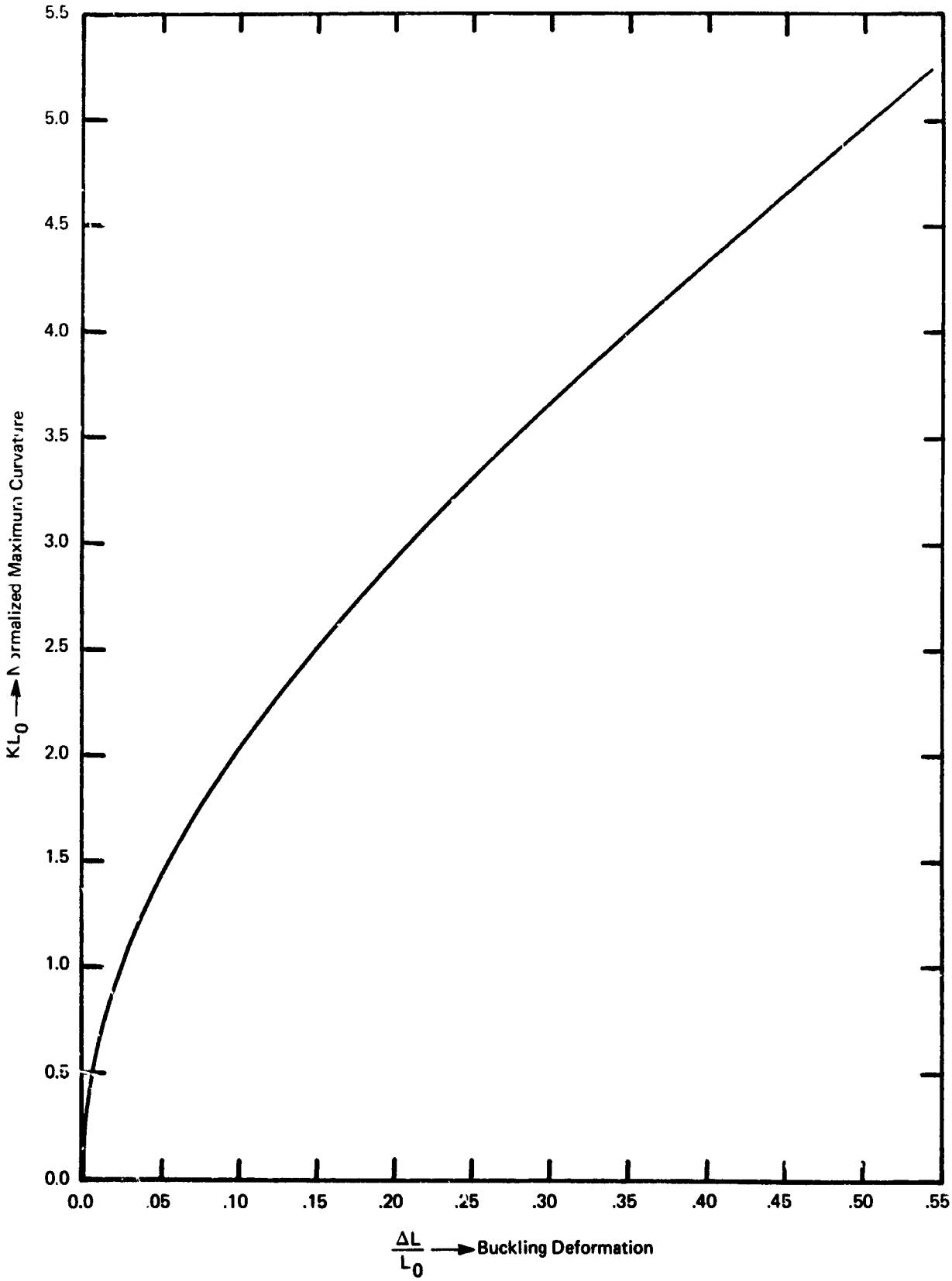

FIGURE 13 NORMALIZED MAXIMUM CURVATURE OF A BUCKLED COLUMN AS A FUNCTION OF NORMALIZED DEFORMATION

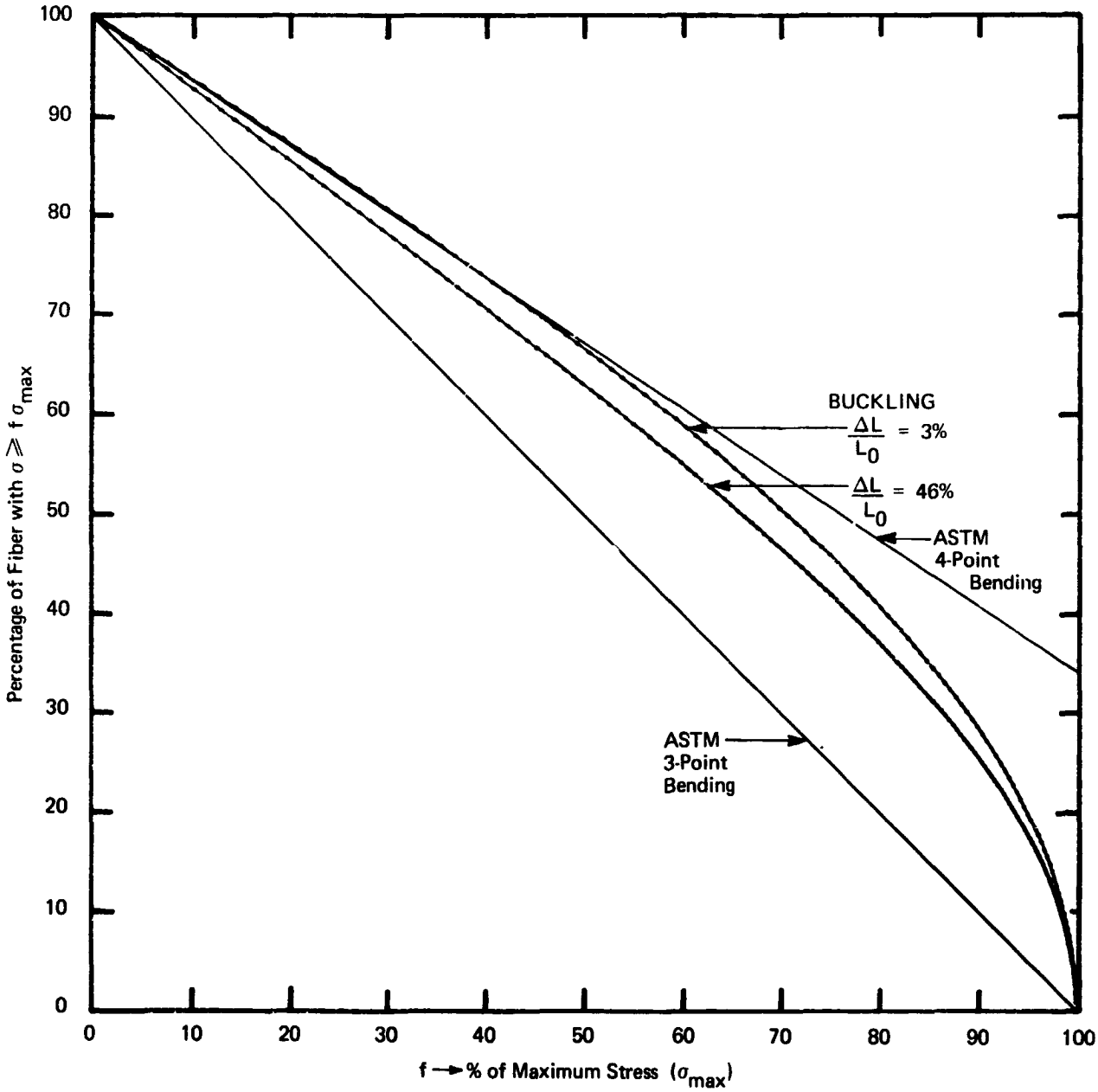

FIGURE 14 COMPARISON OF STRESS DISTRIBUTION IN 3-POINT, 4-POINT AND BUCKLING TESTS

FIGURE 15 SPHEROIDIZED END OF TEST SAMPLE USED IN BUCKLING TESTS. FIBER DIAMETER EQUALS .0325 CM (0.013 IN)

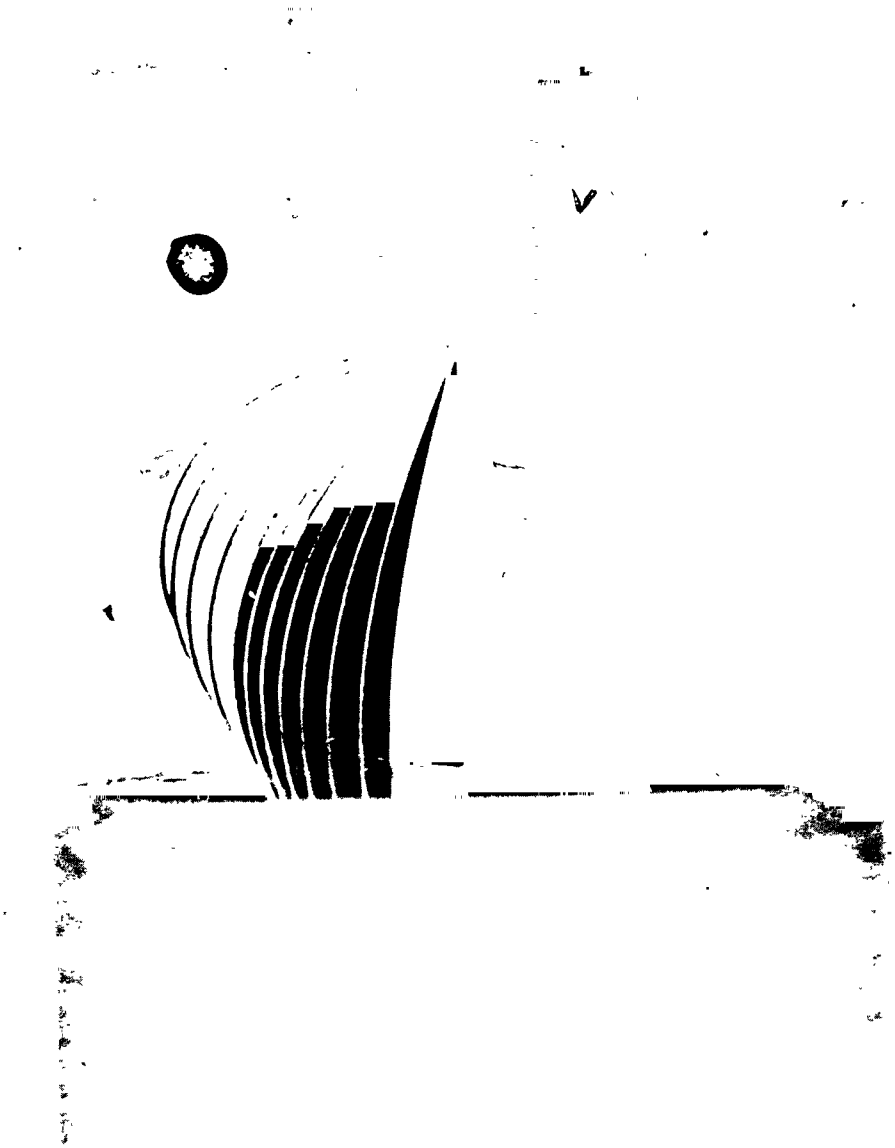

FIGURE 16 INITIAL STAGES OF A FIBER BUCKLING TEST

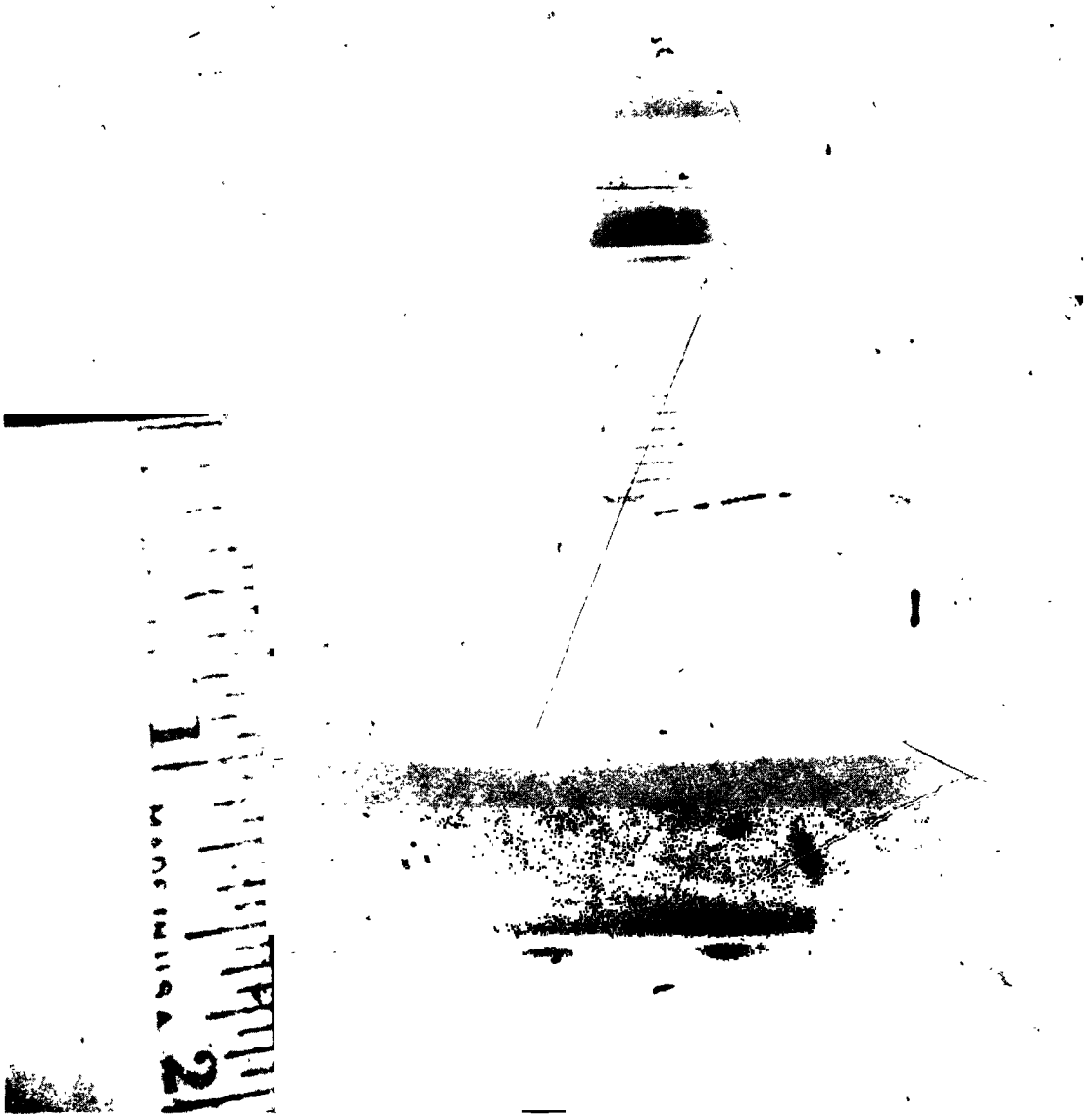

FIGURE 17 Al_2O_3 FIBER (0.033 CM (0.013 INCH) DIAMETER) DEFORMED TO PRODUCE A STRESS LEVEL OF 8.2 X 10^9 N/m^2 (1.19 x 10^6 PSI)

results. Noone, et.al.[6] used a 2.5 cm (1 inch) outer span and 1.25 cm (0.5 inch) inner span in their 4-point bending tests which does not comply with the ASTM test geometry (inner span = 1/3 outer span). The longer-than-standard (approximately 50 fiber diameters) geometry was presumably used attempting to subject a larger sample to high stresses. Our 4-point bending tests used a 5.1 cm (2 inch) outer span and a 1.68 cm (2/3 inch) inner span, since it was anticipated that the diameter of some of the fibers might be as large as 1.10 cm (0.040 inch). We found that the test span was too long for the higher strength fibers. They could sustain such a small radius of curvature that they simply could not be broken. Qualitative evidence of this is shown in Figure 12. This 0.033 cm (0.013 inch) diameter fiber is being bent by hand to a radius of curvature less than 2.5 cm (1 inch) corresponding to a stress greater than $2.7 \times 10^9 N/m^2$ (390,000 psi). The ASTM bending tests use an extremely short gauge length to restrict the amout of new fiber drawn into the jig during deformation. In the case of 4-point bending, the allowed $L-L_o/L_o$ is only 0.2% (L = deformed length, L_o = original span length). In both Noone, et.al's tests and our 4-point bending tests, the $L-L_o/L_o$ for high strength fibers was between 3.5 to 10%. We abandoned the test because it tested a meaningless length of material if the test was done properly and gave potentially erroneous results of the gauge length was extended beyond 6 diameters.

A buckling test was examined as a compromise between the extreme care required to prepare tensile specimens and the simple, but unrepresentatively short sample length of the 4-point bending test. Based on our analyses and the results of the fibers tested to date, we believe that the buckling test meets this goal. The sample preparation and test are simple and reproducible. The sample length can be up to 100 diameters for strengths below $6.9 \times 10^9 N/m^2$ (10^6 psi).

Prior to using this test procedure, buckling of thin elastic columns was examined in detail. In the initial stages of buckling, the shape of the fiber is approximated by a sine-wave. The local stress is similarly described by a sine-wave and therefore has a principal disadvantage of a 3-point bending test; there is only one point in the fiber subjected to a maximum stress. Rather than limit our tests to the domain where a sine-wave approximation is valid, we examined the case for higher levels of deformation. Analytically, we derived an exact solution for the shape of a buckled column without the usual sine-wave approximation. This solution required the solution of elliptical integrals which are tabulated. Our computer solution for the shape of a buckled column used the power series equation which was used to generate the tabulated solutions of elliptical integrals and thus is accurate to approximately six significant figures. Inaccuracies in dimension measurements and other non-uniformities are clearly more significant errors. The curve shown in Figure 13 is the derived solution for the maximum curvature normalized to the fiber length in the fiber ($L_o k$) as a function of cross head displacement normalized to the original fiber length ($\Delta L/L_o$). The maximum stress experienced in the fiber is simply

$$\sigma_{max} = \frac{Er}{\rho} = Ekr$$

where E is the Young's modulus, r is the radius of the fiber and ρ is the minimum radius of curvature survived by the fiber. This is simply taken from Figure 13 by measuring the length (L_o) of the test sample and the crosshead displacement (ΔL) required to break the fiber.

The stress distribution in a highly deformed buckled column differs somewhat from that calculated on the basis of the sine-wave approximation.

For a high $\Delta L/L$, the curvature is distributed more uniformly over the length of the fiber than predicted by the sine-wave solution. contrary to our intuitive thoughts. The distribution of stress in two buckled columns as well as fibers deformed in 3- and 4-point bending are shown in Figure 14. In terms of uniformity of stress, the buckling test is intermediate between the 3-point and 4-point bending tests. For instance, 10% of a fiber deformed in 3-point bending is stressed at 90% or higher than σ_{max}, approxiamtely 20% of a buckled column is in this stress range and 40% of a fiber deformed in 4-point bending is in this stress range. The advantage of the buckling test is that a much larger amount of material can be highly stressed, since the sample length is approximately 100 diameters long rather than only 8. In actual fact, 27 diameters of a fiber are stressed at a level of 90% of σ_{max} or higher in the buckling test, while only 3.2 diameters stressed at this level in a 4-point bending test.

The lengths of buckling samples were set at approximately 100 fiber diameters. With an assumed circular curvature and a maximum stress of $6.9 \times 10^9 N/m^2$ (10^6 psi) this length-to-diameter-ratio produces a semicircle which is the obvious termination point of a buckling experiment.

The ends of the test samples were spheroidized by melting in a acetalene-0_2 flame using a #00 tip. A photograph of a typical spheroidized fiber is shwon in Figure 15. These fibers were then mounted between platens in an Instron testing machine into which spherical depressions had been machined to receive the spherical ends of the fibers. The cross head was raised until a load was noted on the load cell (generally less than 1 to 2 pounds). This point was the reference point from which the change in length at fracture (ΔL) was measured. The initial stages of a buckling experiment are shown in the time-lapse photograph in Figure 16. The extent of the deformation which can be induced in extremely high strength fibers is shown in Figure 17. The maximum tensile stress in this 0.033 cm (0.013 inch) diameter Al_2O_3 fiber is $8.2 \times 10^9 N/m^2$ (1.19×10^6 psi). Comparison of calculated fiber shapes with photographs of deformed fibers shows them to be in excellent agreement.

We believe that the buckling test is a useful testing procedure for materials whose strengths are limited by surface defects. For any assumed strength level, a length-to-diameter ratio can be selected so that the stress is within an arbitrary percentage of the nominal maximum stress over a large fraction of the fiber length. This makes the test a severe test and the large length-to-diameter ratios makes it more representative than 3-point or 4-point bending tests. Comparative results of buckling and tensile tests are given in a later section.

Room temperature tensile testing of the uniform-diameter, high-strength fibers proved troublesome. With fiber strengths up to $2.42 \times 10^9 N/m^2$ (350,000 psi), the piano wire hypodermic tubing grip system[1] appeared adequate. At higher strength levels, the epoxy-adhesive joint was not reliable and many fibers were consumed with pull-outs, fractures at grips and other testing failures. Higher strength fibers were successfully tensile tested (failure away from grips) using an epoxy-tab technique. Fifteen and two-tenth cm (6 inch) long sections of fibers were bonded to a stiff cardboard tab [(2.5x15.2 cm)(1x6 inches)] on which a centerline had been accurately marked. The two ends were covered for 5.0 cm (2 inch) with epoxy leaving a 5.0 cm (2 inch) gauge length ($\ell/d > 140$). The fiber and tab were inserted into convention testing chucks, preloaded, the cardboard sliced at the center and then loaded until the fiber failed. This test procedure was effective, but it obviously was expensive from the standpoint of quantity of fiber consumed per test.

Room temperature tensile testing of the necked samples shown in Figure 11 was straightforward. Either music-wire-hypodermic-tubing or the pin-vice gripping techniques could be used.

b. Elevated Temperature Strengths

All elevated temperature strength measurements were controlled-atmosphere, tensile tests of the reduced cross section fibers according to the geometry shown in Figure 11. The apparatus was that shown in Figure 10. Tests were carried out at 1093 and 1316°C (2000 and 2400°F), respectively. The only exception was TiC. These high temperature strength tests were made in vacuum in the buckling mode.

Gripping, loading procedures and atmosphere control were discussed in Section III.B.2 of this report. The use of reduced cross section samples made these tests straightforward to perform, and with one or two exceptions, all of the fibers broke in their gauge lengths within the hot zone of the furnace.

c. Creep-Rupture Tests

Elevated temperature, long-time failure stress of fibers were carried out in the furnaces described in Section III.B.2. Tests were carried out at 1093 and 1316°C (2000 and 2400°F) in a flowing argon atmosphere. Both uniform diameter and necked sample configurations were used in these tests.

The uniform diameter configuration was suitable only for stress levels below $4.84 \times 10^8 N/m^2$ (70,000 psi). At higher stresses, uniform diameter fibers often failed at their spherodized ends or just out of the hot zone of the furnaces. After numerous attempts to solve gripping problems with the uniform diameter fibers, the necked fiber configuration shown in Figure 11 was used.

The lead-shot weights were supported under the fiber test stations by a bracket attached to a lab-jack, similar to a fork-lift truck. The fibers were first gripped in the upper chuck with the fibers extending through the furnace. The weights were then carefully raised into position and the lower end of the fibers were gripped. Loading was done in repeated steps to allow the weights to approach the centerline before final loading. While the fibers were strong enough to support the loads in tension, twisting or swinging weights caused several fiber failures in early tests.

Precautions were also taken to prevent the laboratory benches, on which the furnaces rested, from being bumped. Despite the fact that the benches were bolted to the floor, were heavily constructed and have 2.5 cm (1 inch) thick slate tops, a small bump, for example from an argon tank, would start the weights swinging. It often took several hours for the swinging to stop.

Other than careful loading and precautions against bumping the benches, the creep-rupture tests presented no serious problem after the necked sample configuration was used. Furnace life may prove a problem if test temperatures raised above 1316°C (2400°F).

2. Results of Fiber Testing

a. Comparison Between Tensile and Buckling Tests

A series of tests were carried out to compare the apparent strengths measured by buckling and tensile tests.

Tensile testing was done with the piano-wire-hypodermic-tubing grip used for all previous tensile testing as well as the so-called epoxy-paper-tab test. Virgin fibers, as well as residual portions of the tensile specimens, were tested in buckling to provide a direct comparison. All of the fibers tested with the piano-wire-tubing jig broke at the tubing; thus, they were not "good" tests. The results of all of the tests were given in Table IV.

Three results are immediately evident. The buckling tests showed that this series of fibers was not as strong as other batches of fibers. The piano-wire-tubing tensile strengths are approximately the same order of magnitude as the best strengths previously measured by this test even though all of these broke at the grips. The epoxy-tab tensile strengths (all broke away from the grips) were substantially higher than the apparent strengths of the piano-wire-tube test. Also, four of these five fibers exhibited higher tensile strengths than have ever been reported for large diameter [(~0.038 cm)(0.015 inch)] Al_2O_3 fibers--whether coated, flame polished or in a controlled atmosphere. All of our tests were made with as-grown, uncoated fibers in a humid atmosphere.

TABLE IV

COMPARISON OF TENSILE AND BUCKLING TEST STRENGTHS

Fiber	Tensile Piano-Wire-Tubing		Tensile Epoxy Tab		Buckling No Previous Test		Buckling Test On Residual of Tensile	
	psi	$N/m^2 x10^{-8}$	psi	$N/m^2 x10^{-8}$	psi	$N/m^2 x10^{-8}$	psi	$N/m^2 x10^{-8}$
59-3			526,500	36.3	695,500	47.9		
60-2	314,000	21.6						
60-2a	223,000	15.3	495,000	34.2			554,000	38.1
60-3	171,000	11.8						
61-2b			pullout		576,000	39.7		
63-3			570,000	39.2			693,000	47.7
63-3a			450,000	21.0				
64-2			265,000	18.3			806,000	55.6

The apparent strengths measured by the buckling test were between 3.45-11.7x10^{8}N/m^2 (50,000-170,000 psi) higher than measured in tension (with the exception of 64-2). The data base is limited, but at this point, it appears that the buckling test gives approximately 6.9x10^{8}N/m^2 (100,000 psi) higher apparent strengths than the epoxy-tab tensile test. It also appears that there is no permanent degradation of the fiber during the tensile test.

The reasons for the higher apparent strengths from the buckling test are understandable. In the buckling test, only one portion of the fiber is subjected to a maximum bending moment and only one side of the fiber is subjected to tensile stresses. It is also clear that the large sample length (~100 diameters) gives a high probability of finding a flaw in the high tensile stress area which is the main reason for the usefuln ss of the test.

The difference between tensile strengths and buck'' strengths gives a qualitative indication of the number of distribution of flaws. If for this batch of fibers an average strength of 4.14x10^{9}N/m^2 (600,000 psi) is assigned to the buckling test and this is compared with 3.45x10^{9}N/m^2 (500,000 psi) observed with tensile tests, it can be seen from the analysis presented in Figure 14 that one serious flaw must occur on the tensile side of the fiber every 30 to 40% of the buckling sample--or 30 to 40 fiber diameters with an ℓ/d = 100. We would not place too much emphasis on this numerical value, but we do believe that it is a good indication that the flaws in these fibers are widely separated. Further evidence of this conclusion is that the two portions of the broken fibers remain intact upon tensile or buckling failure for strengths up to approximately 6.9x10^{9}N/m^2 (10^6 psi). The two fibers which exhibited strengths in excess of 6.9x10^{9}N/m^2 (10^6 psi) totally disintegrated when they failed. By contrast, Tyco fibers disintegrated upon failure when strengths exceeded 1.38-1.72x10^{9}N/m^2 (200-250,000 psi).[7] We believe that this difference in behavior is attributable to the distribution of flaws. All of the Tyco fibers which we have examined contain regularly spaced pores similar to those observed in our earlier fibers. It is widely stated that these pores define the strengths of Tyco fibers since all fracture surface analyses have shown a pore-pore or pore-surface area as the origin of the fracture.[7,8] The strengths of Tyco fibers are quite uniform, and the strain energy at the point of fracture is high enough to cause the remainder of the fiber to break up. Ours appear to be generally much stronger, but they contain widely distributed serious flaws which probably result from the batch nature of the process.

The most important result of these tests is that they show that the buckling test does give an accurate measure of fibers' strengths. Thus, to our knowledge, the Al_2O_3 fibers which supported stresses in excess of 6.9x10^9 N/m^2 (10^6 psi) are probably the strongest bulk fibers ever grown.

b. Al_2O_3

In the early phase of the program (Task II), Al_2O_3 single crystal fibers were grown under a variety of growth conditions and from different feed

rod compositions. A summary of the test results accumulated at the end of Task II is given in Table V. Following this period, Al_2O_3 fibers were grown only from Linde material to produce needed test specimens. It was explicitly stated that our objective was not one of optimizing growth conditions and properties of Al_2O_3 fibers.

All of the fibers grown from commercial grade feed rods were substantially weaker than those grown from the higher purity Linde feed rods; they also generally exhibited the chevron surface traces and related internal pores observed by us in previously grown fibers[1] and in Tyco fibers.[8] A chemically polished fiber exhibiting this characteristic is shown in Figure 18. In this case, the surface of the large diameter region below the neck was not etched, thus, represents the as-grown surface. It is evident that the defects extend throughout the volume of the fibers as reported previously.[1] This defect structure is believed to be caused by the loss of solidification-interface stability.

The differences between the strengths of fibers grown from commercial grade feed materials and those grown from higher purity feed rods is believed to be related to the high concentrations of specific impurities shown in Table II. In other work, we have grown fibers from high purity, low density polycrystalline feed rods and from repeatedly zone refined commercial feed rods which equaled the best fibers grown under this program. Thus, the same quality fibers can be expected from continuously-extruded, low density feed rods.

Subsequent batches of Cr-doped Al_2O_3 test fibers exhibited average strengths between approximately $4.15 \times 10^9 N/m^2$ (600,000 psi) and $5.5 \times 10^9 N/m^2$ (800,000 psi). The lowest measured strength was $2.83 \times 10^9 N/m^2$ (410,000 psi) and the highest was $9.65 \times 10^9 N/m^2$ (1,400,000 psi). These strengths were based on an assumed Young's modulus of $4.15 \times 10^{11} N/m^2$ (60×10^6 psi). Recently, the modulus of C-axis Al_2O_3 fibers and ribbons was reported to be $4.7 \times 10^{11} N/m^2$ (67.5×10^6 psi).[8] Thus, these strengths might actually be proportionally higher, since strengths were measured by measurement of radius of curvature at the point time failure.

Based on the results of these room temperature strength measurements, it is clear that the CO_2 laser-heated, floating zone fiber growth process has significantly advanced the state-of-the-art in production of high strength fibers. These bulk fibers have strengths which had only previously been observed in single crystal whiskers.

The results of the high temperature tensile tests are shown in Figure 19 and summarized in Table VI. The sample geometries of the 0.028 and 0.048 cm (0.011 and 0.019 inch) diameter fibers were those shown in Figure 11. The most recent high temperature tensile strengths reported by Tyco[9] are included in Figure 19 for comparison.

In addition to the strengths Tyco reported,[9] Crane and Tressler[10] and Shahinian[3] have recently reported high temperature tensile strength measurements with 0.025 cm (0.010 inch) diameter Tyco fibers. Their results are in close agreement but are higher than the strengths reported by Tyco. Approximate tensile strengths for these fibers were $7.6 \times 10^8 N/m^2$ at 1093°C (110,000 psi at 2000°F) and $5.65 \times 10^8 N/m^2$ at 1316°C (82,000 psi at 2400°F).

TABLE V

STRENGTHS OF Al_2O_3 FIBERS

	Fiber Diam. (in)	Fiber Diam. (cm)	Type of Test	Strength (psi)	Strength ($N/m^2 \times 10^{-8}$)
Coors-995 Single Pull up in air	0.0202	0.051	4 pt	108,800	7.44
Coors-995 Single Pull down in air	0.0188	0.048	4 pt	90,000	6.20
Coors-995 Double Pull up in air	0.0205	0.052	4 pt	17,300	1.17
Coors-995 Double Pull down in air	0.0180	0.046	4 pt	86,600	5.96
Degussa AL-23 Single Pull up in air	0.0202	0.051	4 pt	117,900	8.12
Degussa AL-23 Single Pull up in air	0.0186	0.047	4 pt	245,175	16.90
Degussa AL-23 Single Pull up in air	0.0186	0.047	4 pt	23,350	1.62
Degussa AL-23 Single Pull down in air	0.0175	0.046	4 pt	13,000	0.90
Degussa AL-23 Single Pull down in Ar-5%H_2	0.0301	0.077	B	304,200	21.00
Degussa AL-23 Single Pull down in Ar-5%H_2	0.0182	0.046	B	294,300	20.20
McDanel AP-35 Single Pull up in air	0.0265	0.067	4 pt	151,000	10.40
McDanel AP-35 Single Pull down in air	0.0302	0.077	4 pt	48,900	3.37
McDanel AP-35 Single Pull down in Ar-5%H_2	0.0212	0.054	B	181,260	12.46
McDanel AP-35 Double Pull down in air	0.0196	0.050	4 pt	29,800	1.98
McDanel AV-30 Single Pull down in air	0.0230	0.059	4 pt	24,600	1.70
Linde Single Pull down in vacuum	0.0226	0.057	T	>330,275	>22.75
same sample	0.0226	0.057	B	110,870	7.60
Linde Single Pull down in vacuum	0.0226	0.057	B	320,000	22.05
Linde Single Pull down in vacuum	0.0226	0.057	B	331,500	22.80
Linde Single Pull down in vacuum	0.0218	0.055	T	307,800	21.15
same sample	0.0218	0.055	B	279,540	19.20
Linde Single Pull down in vacuum	0.0218	0.055	B	435,500	30.00
Linde Single Pull down in vacuum	0.0200	0.051	T	>168,000	>11.55
same sample	0.0200	0.051	B	431,000	29.70
Linde Single Pull down in vacuum	0.0200	0.051	B	703,800	48.40
Linde Single Pull down in vacuum	0.0200	0.051	B	990,000	68.20
Linde Single Pull down in vacuum	0.0209	0.053	T	>140,000	> 9.65
same sample	0.0209	0.053	B	329,730	22.65
Linde Single Pull down in vacuum	0.0200	0.051	B	196,200	13.50
Linde Double Pull down in vacuum	0.0216	0.055	B	449,000	30.90
Linde Double Pull down in vacuum	0.0137	0.035	B	>1,195,000	>82.40
Linde Double Pull down in vacuum	0.0134	0.034	B	1,286,000	88.50
Linde Double Pull down in vacuum	0.0134	0.034	B	995,750	68.60
Linde Double Pull down in vacuum	0.0166	0.042	T	>260,000	>17.90
same sample	0.0166	0.042	B	132,160	9.10
Linde Double Pull down in vacuum	0.0132	0.033	T	244,000	16.80
same sample	0.0132	0.033	B	185,340	12.70

4 pt. - 4-point bending
B - buckling
T - Tensile

FIGURE 18 PHOTOGRAPH OF CHEMICALLY POLISHED Al_2O_3 FIBER GROWTH FROM COORS 995 (PINK) 44X

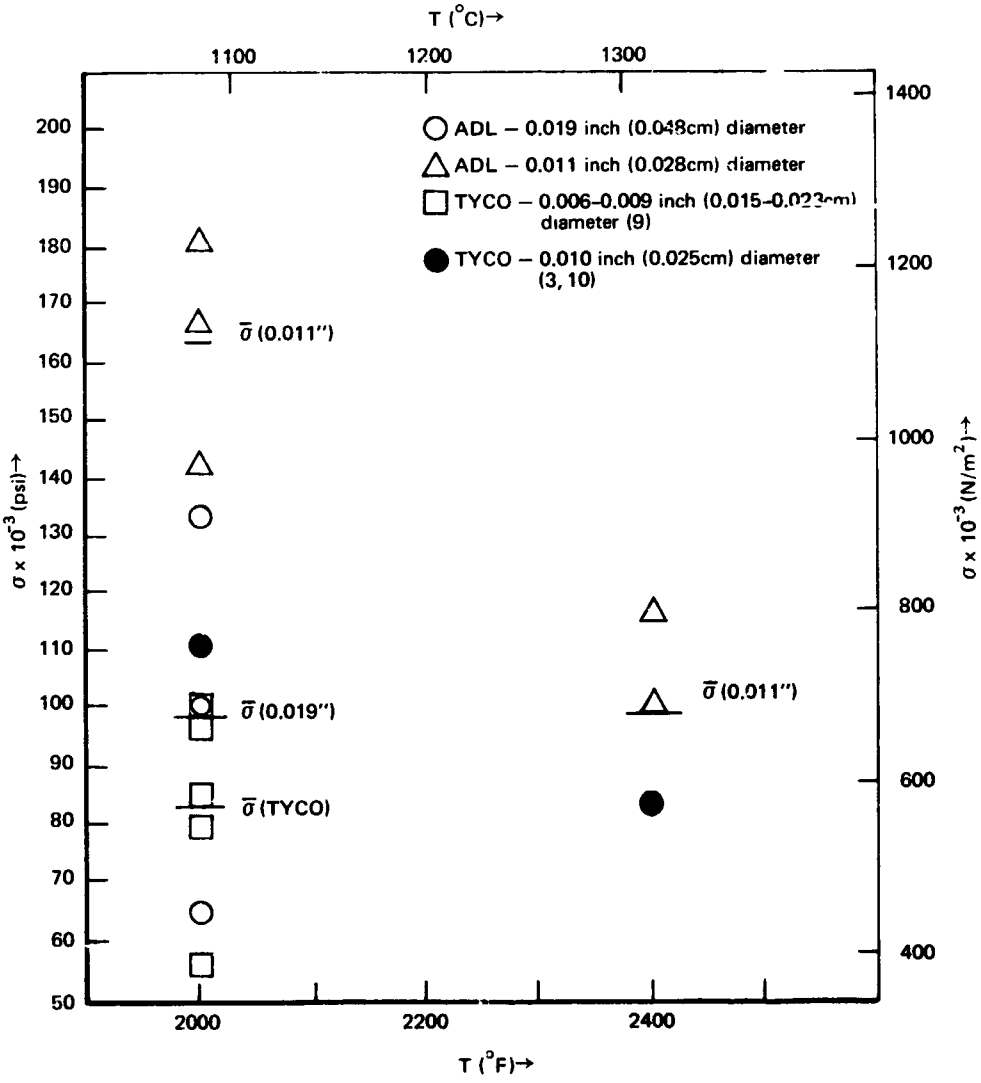

FIGURE 19 HIGH TEMPERATURE STRENGTHS OF Al_2O_3 FIBERS MEASURED IN TENSION. THE LINES DENOTED BY $\bar{\sigma}$ REPRESENT THE AVERAGE STRENGTHS FOR EACH FIBER TYPE.

TABLE VI

RESULTS OF ELEVATED TEMPERATURE TENSILE TESTS

Sample No.	Gauge Diameter		Test Temperature		Tensile Strength	
	(in)	(cm)	(°F)	(°C)	(psi)	(N/m^2)
94-1	0.019	0.048	2000	1093	133,000	9.15×10^8
94-3	0.019	0.048	Broke on Handling			
94-2	0.019	0.048	2000	1093	65,000	4.47×10^8
94-4	0.019	0.048	Broke on Handling			
94-5	0.019	0.048	2000	1093	100,000	6.9×10^8
95-2	0.019	0.048	Broke on Handling			
				AVERAGE =	99,330	6.85×10^8
96-2	0.0120	0.030	2000	1093	180,000	12.4×10^8
95-5	0.0110	0.028	2000	1093	166,000	11.4×10^8
95-3	0.0115	0.029	2000	1093	142,000	9.8×10^8
				AVERAGE =	162,666	11.2×10^8
96-3	0.012	0.030	2400	1316	116,000	8.0×10^8
96-1	0.0115	0.029	2400	1316	110,000	7.6×10^8
95-4	0.010	0.028	2400	1316	101,000	6.9×10^8
				AVERAGE =	109,000	7.5×10^8

The horizontal bars denoted by $\bar{\sigma}$ represent the average strengths for each group of fibers.

These results show that the strengths of Cr-doped, C-axis Al_2O_3 fibers exceed the program's goal, which was $6.9 \times 10^8 N/m^2$ at 1093°C (100,000 psi at 2000°F), since these fibers exhibited an average strength in excess of $6.9 \times 10^8 N/m^2$ at 1316°C (100,000 psi at 2400°F).

A size effect on fiber strength is apparent. At 1093°C (2000°F) the average strengths of 0.048 cm (0.019 inch) diameter fibers were approximately 60% of the average strength exhibited by the 0.028 cm (0.011 inch) diameter fibers. Based on these limited results, we would not attribute the difference entirely to size of the fibers. Fibers of both diameters were grown with identical optical-bench adjustments; so it is probable that the growth conditions were not optimized for either fiber diameter. Thus, even though the relationship between sample size and strength is well known, some of the difference may be attributable to less-than-optimum growth conditions for the 0.048 cm (0.019 inch) diameter fibers.

The ADL and Tyco growth processes and compositions are different, so it is not possible to state with any certainty why ADL fibers are stronger at elevated temperatures. The room temperature tests, however, do show that the ADL fibers are superior from the standpoint of flaws. The temperature dependence of strength is qualitatively the same for all reported measurements. The strengths at 1316°C (2400°F) are between 67 to 75% of the 1093°C (2000°F) levels. If some type of microplastic deformation is responsible for the apparently brittle fractures at these elevated temperatures, then the Cr doping is probably responsible for the increased strengths. It is well known that Cr and other dopants raise critical resolved yield stresses in Al_2O_3.[11]

Limited examination of Al_2O_3 fiber fracture surfaces in this program revealed that the room temperature failure mechanism is apparently different from that operative in the 1093 to 1316°C (2000 to 2400°F) range. Scanning electron microscope examination of room temperature fracture surfaces revealed no preferred cleavage plane and generally showed failures originating at exterior surfaces. This characteristic behavior is shown in Figure 20 which is a fiber that failed at $3.98 \times 10^9 N/m^2$ (576,000 psi) in tension at room temperature. On elevated temperature test samples, well defined cleavage faces were always evident. In all cases, the cleavage planes were identified to be perpendicular to $[\bar{1}102]$ poles. Several fibers exhibited all three planes intersecting within the fiber. Charles and Shaw[12] reported similar fracture surfaces on undoped Al_2O_3 when tested in air or wet atmospheres.

We have not studied the short time strength-controlling mechanisms in C-axis Al_2O_3 fibers beyond this limited extent. These preliminary observations do suggest that the strength-limiting fracture-mechanism changes with temperature; thus, it is obvious that the subject warrants further study if strengths are to be increased.

The results of 1093 and 1316°C (2000 and 2400°F) creep-rupture tests with Al_2O_3 fibers are shown in Figures 21 and 22, respectively. Stresses were normalized to specific stresses (σ/ρ), since this is the important materials parameter for rotating apparatus, such as turbine blades. Actual stress levels vary from 3.65×10^8 to $6.2 \times 10^8 N/m^2$ (53,000 psi to 90,000 psi). The specific 1093°C(2000°F) creep-rupture properties of W and W-2% ThO_2 fibers are also plotted on Figure 21 for comparison with the performance of these fibers. In terms of high temperature creep-rupture properties, these W-2% ThO_2 filaments are the highest performance materials reported to date. The C-axis, Cr-doped Al_2O_3 fibers represent approximately a four-fold improved performance at 1093°C (2000°F). No data is available for W-2% ThO_2 at 1316°C (2400°F), so we cannot make a comparison of properties at the higher temperature. Comparison of the long-time strengths exhibited by ADL Cr-doped Al_2O_3 fibers at the two temperatures shows that within the accuracy of the limited date, the creep-rupture strengths have not dropped significantly between 1093 and 1316°C (2000 and 2400°F).

These tests proved extremely troublesome at stress levels in excess of $4.8 \times 10^8 N/m^2$ (70,000 psi) until the necked sample configuration was adopted. Approximately 25 test samples broke in grip regions either during or shortly after loading. Many other fibers pulled out of grips and were damaged.

The data points denoted by an asterisk on Figures 21 and 22 represent stresses and times-of-failure, but are considered suspect. For instance, Fiber 64-3A survived $5.5 \times 10^9 N/m^2$ (80,000 psi) loading at 1093°C (2000°F) for 400 hours. The furnace was shut down at this point, since the fibers in the other three furnace stations had broken out of the hot zones of the furnaces. This fiber broke within one hour of reloading after the other stations were filled with samples. We believe that the fiber would have survived longer if it had not been disturbed. The fiber did not break in hot zone of the furnace which is further reason to suspect the validity of the result.

Three other uniform diameter fibers broke within the furnaces; however, the validity of all of the results is questionable. Fibers loaded at $5.5 \times 10^9 N/m^2$ [(80,000 psi)(#83-2)] and $4.96 \times 10^9 N/m^2$ [(72,000 psi)(#85-1a)] broke after 16 and 113 hours, respectively, at 1093°C (2000°F). Both fibers broke above the hot zones of the furnaces. Fiber #86-4, loaded at $5.16 \times 10^9 N/m^2$ (75,000 psi) broke after 24 hours at 1316°C (2400°F), again above the hot zone. The consistence of failures at 4.8×10^9 to $5.5 \times 10^9 N/m^2$ (70,000 to 80,000 psi) above the hot zone of the furnaces with the previously reported minimum in the tensile strength of sapphire at approximately 500°C (930°F) is striking. All subsequent tests were made with the necked sample configuration.

Only one of these fibers has failed at the time of report preparation. This fiber failed after 24 hours stressed at $6.2 \times 10^9 N/m^2$ at 1093°C (90,000 psi at 2000°F). All other samples are still running at the time of report preparation. These data points are denoted by arrows. The tails of the arrows are the accumulated loaded time at the date of report preparation.

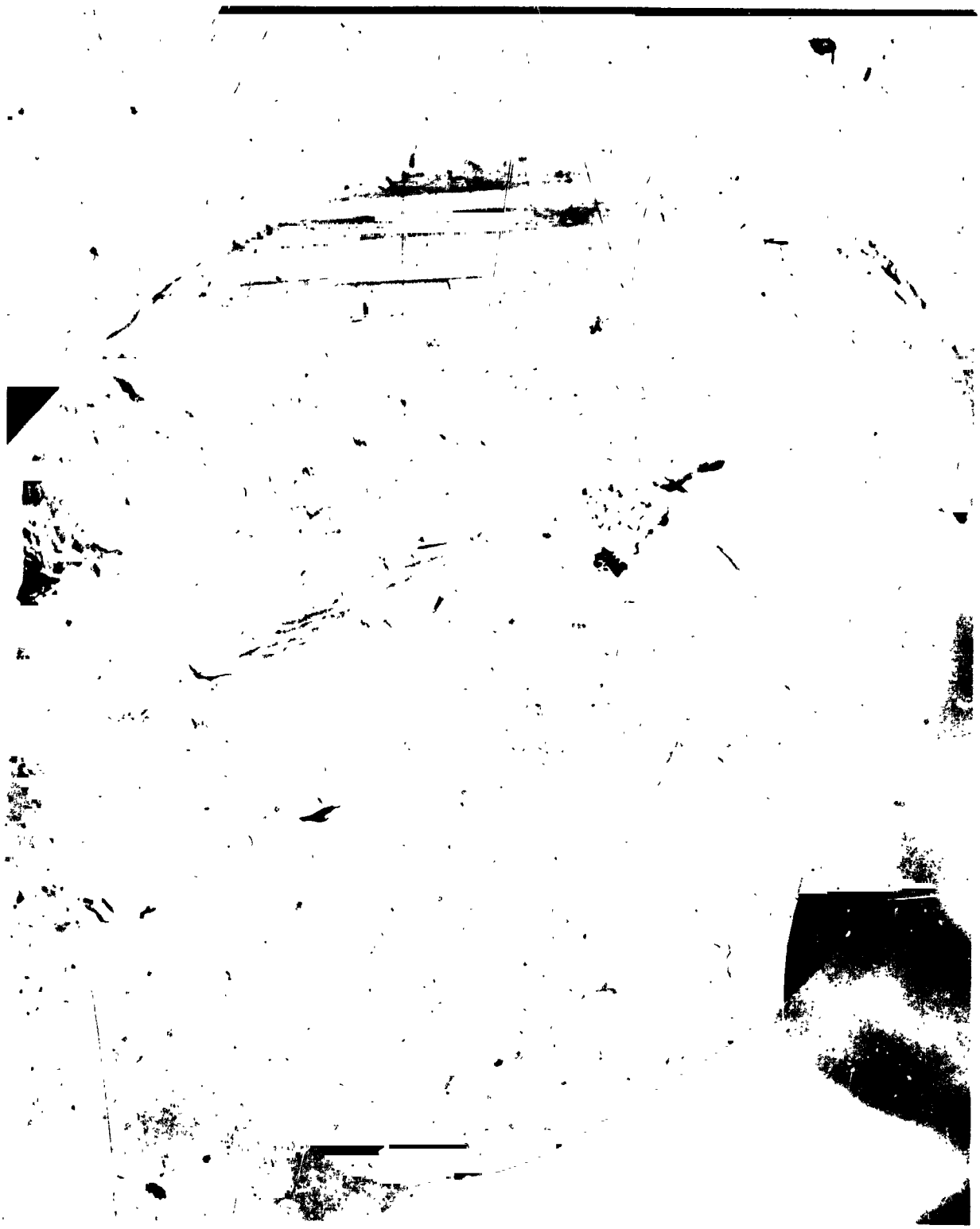

FIGURE 20 FRACTURE SURFACE OF Al_2O_3 FIBER 61-2B WHICH EXHIBITED A TENSILE STRENGTH OF 39.6×10^7 N/m^2 (576,000 PSI) MAGNFICATION 580X

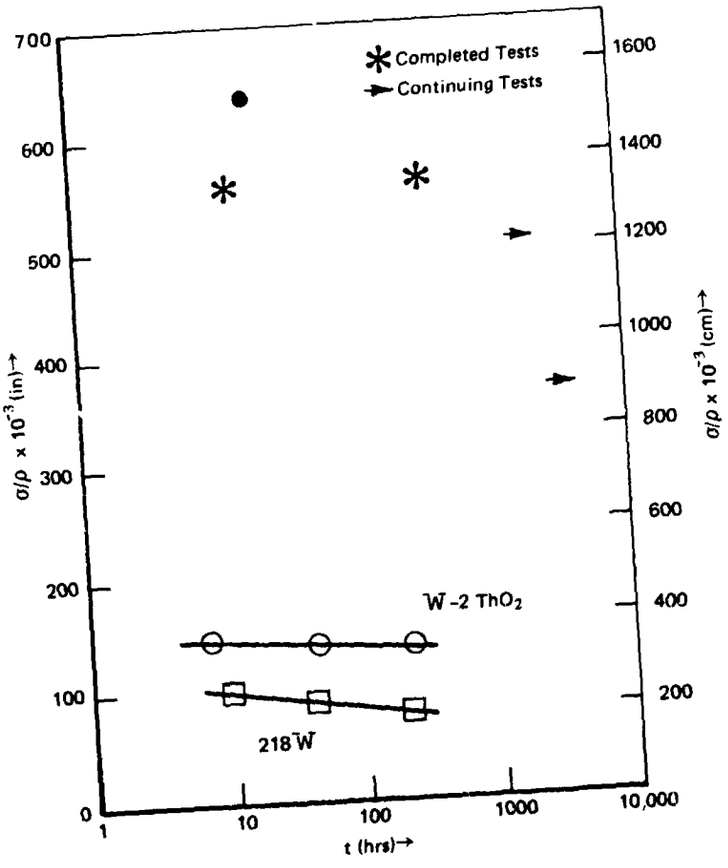

FIGURE 21 SPECIFIC CREEP-RUPTURE RESULTS FOR ADL Al_2O_3 FIBERS AT 2000°F (1093°C)

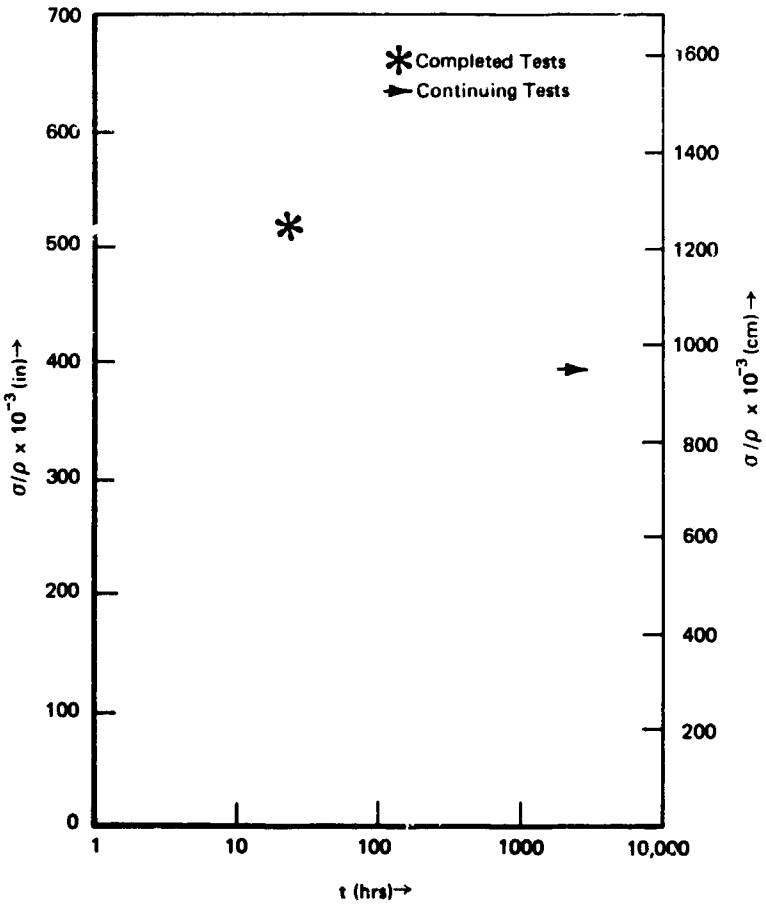

FIGURE 22 SPECIFIC CREEP-RUPTURE RESULTS FOR ADL Al_2O_3 FIBERS AT 2400°F (1316°C)

The mechanism responsible for delayed failures (creep-rupture) of these fibers is not known. Scanning electron microscopy has revealed no evidence of slip lines or of other surface degradation such as thermal etching of low angle grain boundaries or dislocations. All of the fibers have developed surface stains in the regions enclosed by the furnaces, but not necessarily in the hot zone regions. The stains have not been identified. The coatings evidently are quite conductive since the fibers can be studied in the SEM without charging effects without using the usual carbon and gold coatings required with insulators.

Even with the questions concerning the validity of the long-time, high temperature strengths, these C-axis, Cr-doped Al_2O_3 fibers exceed the performance of all competitive materials. With one exception, these data points probably represent lower than true strengths, either because of reactive interactions with furnace materials (stains) or handling during tests. The implication of these results for probable composite performance will be discussed later; however, rule-of-mixture composite properties would permit significantly improved materials.

c. Y_2O_3

All of the Y_2O_3 single crystal fibers have been extremely high quality from the standpoint of microstructural and surface defects in the as-grown condition. This observation is made based on the unusually good light-piping effect evident in all growth runs. Any internal flaws (precipitates, pores, cracks, etc.) or surface flaws are visible during growth, since the molten zone acts as an intense dark field illuminator, and their presence is indicated by a decreased intensity of light transmitted down the fiber. Thus, these fibers had the potential of achieving high strengths since they appeared to be free of structural defects.

All of the first several fibers cracked spontaneously during growth. Cracking appeared to occur at a fixed position relative to the molten zone. X-ray Laue analyses showed that all fibers were single crystal, no preferred growth axis was exhibited, and the cracks did not follow specific crystallographic planes.

In one case, after approximately 5.1 cm (2 inches) of growth, the spontaneous cracking stopped. When this uncracked fiber was used as a seed for subsequent growth runs (growth axis approximately 14° from a <100> axis), spontaneous cracking did not occur. Elimination of spontaneous cracking in these fibers probably was not related to the specific growth axis, since fibers with the same growth axis exhibited spontaneous cracking during growth. Rather, it probably resulted from initiating growth from crack-free material. We have observed similar behavior in several high temperature gradient, crystal growth processes. It appears that stable cracks exist in the growing crystals and they propagate at the rate of growth. In all cases, crack-free crystals could be grown from crack-free seeds.

After exposure to room atmosphere for at least 24 hours, all of these crack-free Y_2O_3 single crystals spontaneously cracked into sections approximately

2 diameters long. Y_2O_3 fibers which were stored up to 4 months (age of fibers at date of report preparation) in a desicator ($CaSO_4$) have not exhibited this spontaneous cracking. Apparently, Y_2O_3 is extremely susceptible to a water-enhanced stress corrosion or other degradation mechanism.

Mechanical testing of the Y_2O_3 single crystal fibers was limited to room temperature buckling tests. Maximum tensile strains at failure were approximately 3.4×10^{-3} [cm/cm] or [in/in]. The reported elastic modulus of Y_2O_3 was $1.1 \times 10^{11} N/m^2$ (16.6×10^6 psi), but it was doubted because the unsubstantiated reference[13] was old and the value did not follow the typical correlation with melting point and modulus. The Young's modulus of single crystal Y_2O_3 fibers, measured in 4-point bending, was between 1.07×10^{11} to $1.1 \times 10^{11} N/m^2$ ($15\text{-}16 \times 10^6$ psi). Thus, room temperature strengths were approximately $3.86 \times 10^8 N/m^2$ (56,000 psi). It should be noted that these tests were conducted in room atmosphere, so it is probable that the observed water vapor enhanced degradation mechanism effected the observed strengths.

Further experiments with Y_2O_3 were abandoned due to the unacceptably low modulus of elasticity. The apparent susceptability to water vapor was not a prime factor in reaching this decision, but it would clearly make it difficult to handle and process the fibers.

d. TiC

The number of mechanical property measurements with TiC single crystal fibers were limited because only a few "good" samples were available. All of these were uniform in diameter and thus were not suited to high temperature tensile tests. Room temperature strengths were measured in 4-point bending and high temperature strengths in buckling. The buckling test was not used for room temperature tests because the ends of the fibers could not be spherodized by flame melting. It was feared that non-spherical ends would cause spurious results. The buckling test was used at high temperature because of available equipment and time limitations even though it was recognized that the non-spherical ends were not desirable.

The room temperature strengths of three TiC single crystal fibers (#79-1, #80-2, #81-1) were 1.54×10^9, 1.52×10^9 and $0.87 \times 10^9 N/m^2$ (224,000, 221,000 and 127,000 psi), respectively. The two higher strength fibers had shiny, metallic surfaces. Fiber 81-1 had a shiny, but stained, surface. All fiber diameters were approximately 0.0635 cm (0.025 inch). Fibers 80-2 and 81-1 were grown along <111> axes. Fiber 79-1 was unseeded and grew within 14° of a <110> axis.

At 1093°C (2000°F), Fiber 80-2 had a strength of $5.05 \times 10^8 N/m^2$ (73,000 psi). Several other TiC fibers were broken unintentionally while heating to the test temperature because the sliding friction of the push rods into the W-mesh-basket, vacuum furnace was higher than the load required to buckle and fracture the samples. Thus, we were not able to determine when a load was applied to the fibers until the furnace reached red-heat and the fibers became visible. Testing was not pursued further due to the limited number of available samples, the difficulty of testing, and the poor quality of the feed rods.

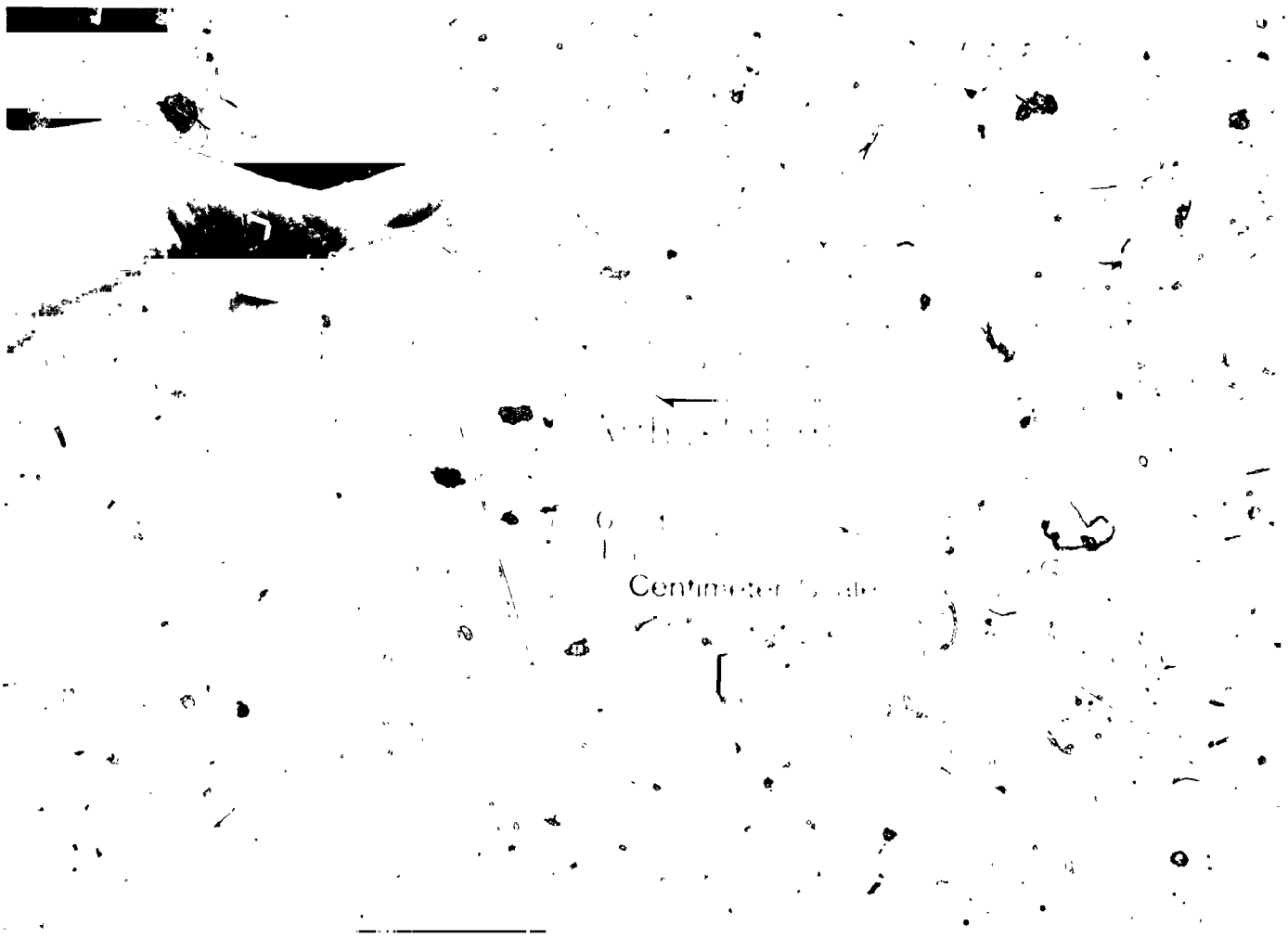

FIGURE 23 TiC SINGLE CRYSTAL FIBER

FIGURE 24 FRACTURE SURFACE OF A TiC SINGLE CRYSTAL FIBER WHICH EXHIBITS {100} CLEAVAGE PLANES MAGNIFICATION 800X

C.2

As discussed in an earlier section, the Si contamination level was so high in these feed rods that free SiO_2 was present. Often, growth would proceed smoothly for 2.5 cm (1 inch) or more and then suddenly the molten zone would burst as if something had vaporized rapidly, such as SiO_2 particles at approximately 3200°C (5800°F). In some cases, growth proceeded with continuous, but less violent, vaporization from the zone which produced rough surfaces. The TiC fiber shown in Figure 23 was one of the few that grew essentially the full stroke-length without interruption. It appeared that additional testing was not warranted until higher quality feed materials became available.

The strengths observed with these TiC fibers are extremely promising despite the conditions under which they were grown and tested. All of the cited factors could only reduce apparent strength levels. Both room temperature and elevated strengths were higher than ever achieved during the first year's program[1] and were stronger than many of the Al_2O_3 fibers grown early in this program (Table V). The specific strength observed at 1.08×10^6 cm at 1093°C (410,000 in at 2000°F) exceeds the specific 1093°C (2000°F) strength of W-2%ThO_2 wire [(approximately 402,000 cm (158,000in)][14] which is considered a prime candidate for reinforcement of metal matrix composites. The specific TiC fiber strength also essentially equaled the specific 1093°C (2000°F) strength of SiN and SiC[15][(952,000-1.080,000cm) (375,000-425,000 in)] which are considered two of the most promising high temperature structural materials. There is good evidence that the TiC fiber strengths can be improved by more controlled fiber growth conditions as well as using dopants (B) and/or alloying elements (V).[16]

All of the TiC filaments failed brittlely by cleavage on {100} planes. In some cases the fracture surfaces were made up of predominantly {100} steps as shown in Figure 24, but generally they were very flat. We observed no evidence of plastic deformation at room or elevated temperatures. The fracture mechanism appeared to be brittle cleavage in all cases. As is the case with the Al_2O_3 fibers, understanding and controlling the cleavage-mode of fracture appears fundamental to achieving substantially improved high temperature strengths.

IV. SUMMARY OF RESULTS

In terms of the program's goal of using the CO_2 laser heated floating zone fiber growth process to grow fibers of materials that were not previously available and to grow fibers under conditions which are not accessible to other process, the program has been entirely successful. While it was explicitly intended that the program was to be a materials survey program, substantially improved room temperature and high temperature mechanical properties were achieved without attempting optimization of growth procedures. Relatively little effort was made analyzing modes of failure and otherwise characterizing fibers. The majority of the program's effort was devoted to assembling a unique apparatus, learning how to grow fibers of several different materials, testing the fibers, and based on these results, modifying the growth procedures and apparatus.

The principal result of the previous program was that this fiber growth process worked according to the predictions of extensive analyses. Absolute stability existed over wide ranges of attenuation ratios and an inherent kinematic stability produces excellent dimensional uniformity. At that time, room and elevated temperature strengths did not equal state-of-the-art values.

This deficiency was resolved during this program. The room temperature strengths exhibited Cr-doped Al_2O_3 fibers [(up to $9.65 \times 10^9 N/m^2$)(1.4×10^6 psi)] had only been observed previously with small, "whisker" single crystals. The high temperature properties of these fibers were equally impressive, particularly the specific creep-rupture strengths. One hundred-hour specific creep-rupture strengths are in excess of 1,400,000 cm at 1093°C (550,000 in at 2000°F) and 1,205,000 cm at 1316°C (475,000 in at 2400°F). Precise values cannot be given because of the limited data. These specific 1093°C (2000°F) creep-rupture results represent an approximate four-fold improvement over any previously published results. The 1316°C (2400°F) specific creep-rupture results have no significant base for comparison, since the properties reported for potentially useful fiberous materials have deteriorated for unusable values by this temperature. Materials, such as boron, carbon and SiC, retain high strengths at these temperature levels; however, their extreme reactivity with all potential matrices and extreme surface sensitivity makes them dubious candidates for this temperature range. The program's strength goal [($6.9 \times 10^8 N/m^2$)(100,000 psi)] was reached 220°C (440°F) higher than sought [(1093°C) or (2000°F)]. These results demonstrate that extremely high quality fibers can be grown by the floating zone fiber growth process.

Growth of TiC single crystal fibers demonstrate one of the unique capabilities of the process-producing fibers from melts for which no known crucible material exists. Growth of Cr-doped Al_2O_3 fibers under extremely

oxidizing conditions demonstrates a second unique feature--growing fibers from melts under conditions which are inaccessible to other processes. While the strengths of the TiC fibers were not as high as the best Al_2O_3 fibers, they were extremely promising. These results combined with the low density of TiC indicate that it must be seriously considered for reinforcement of metal matrix composites. Utilization of the second feature permitted retention of high Cr levels in Al_2O_3 fibers which was undoubtedly responsible for their extremely good high temperature properties.

The specific stress levels under which a competitive composite materials must operate are 127 to 177×10^3 cm (50 to 70×10^3 in) for 1000-hour creep rupture.[14] With current superalloys, the upper, uncooled blade temperature limit is in the range of 980-1040°C (1800-1900°F).[15] Metal-matrix composites based on W-2%ThO_2 fibers may be expected to raise uncooled blade operating temperatures to approximately 1150°C (2100°F), since their 1000-hour creep-rupture strengths are approximately (probably greater than) $4.2 \times 10^8 N/m^2$ (61,000 psi) at this temperature. Based on a non-load-bearing metal matrix (specific gravity = 8.9) reinforced with 30 volume percent Al_2O_3 fibers (specific gravity = 4.0), a 1000-hour fiber strength of approximately $3.04 \times 10^8 N/m^2$ (44×10^3 psi) is required to produce composites with useful 1000-hour creep-rupture lives. TiC fibers (specific gravity = 4.93) must have 1000-hour strengths of approximately $4.5 \times 10^8 N/m^2$ (65×10^3 psi) to produce a composite with the same performance. These values have already been exceeded.

There are clearly many problems to be overcome before operation at these temperature levels can seriously be considered; however, this program has produced fibers which can easily meet the high-temperature property requirements. The TiC filaments are not yet strong enough to permit markedly increased performance conditions, but their properties demonstrate a high probability of reaching the required levels. It should be emphasized that it was not our objective to optimize growth conditions with any of these materials. From the technical literature, there is every reason to believe that substantially improved properties can be achieved with Al_2O_3 and TiC fibers by the use of selective dopants and/or alloying agents.

ACKNOWLEDGEMENTS

The team which conducted this program was made up of several ADL staff members. Misters P. VonThuna and L. Lapson were responsible for the design of the optical system. Mr. M. Rossetti participated in designing and building the mechanical testing apparatus as well as carrying out much of the testing. Dr. A. Emslie and Mr. P. Strong conducted the analysis of the buckled column. Mr. L. Lindonen was responsible for carrying out most of the fiber growth runs.

Their contributions are greatfully acknowledged.

REFERENCES

(1) J. S. Haggerty and W. P. Menashi. Production of Oxide Fibers By a Floating Zone Process. Final Report NAS 3-13479, February 1971.

(2) Dr. Joseph Richmond. National Bureau of Standards. Private Communication.

(3) P. Shahinian, J. Amer. Ceram. Soc. 54, 67 (1971).

(4) E. A. Jackson and J. P. Roberts, Trans. Brit. Ceram. Soc. 54, 389 (1955).

(5) J. B. Wachtman and L. H. Maxwell, J. Amer. Ceram. Soc. 42, 432 (1959).

(6) M. J. Noone, et. al., Development of Composite Structural Materials For High Temperature Applications, Naval Air Systems Command Final Report, Contract N00019-68-C-0304, December 18, 1967.

(7) R.L. Crane, WPAFB, Dayton, Ohio. Private Communication.

(8) G. F. Hurley and F. T. A. Pollock. Met. Trans. 3, 397 (1972).

(9) Sapphire Filaments, G. F. Hurley and F. T. A. Pollock AFML-TR-71-13 Part I.
AFML-TR-71-13, February 1971.

(10) R. L. Crane and R. E. Tressler, J. Composit. Mat. 5, 537 (1971).

(11) K. C. Radford and P. L. Pratt, Pro. Brit. Ceram. Soc. 15, 185 (1970).

(12) R. F. Charles and R. R. Shaw. Delayed Failure of Polycrystalline and Single Crystal Alumina
General Electric Report No. 62-RL-3081M July 1962, Published by the Research Information Section, The Knolls, Schenectady, N. Y.

(13) E. K. Keler and A. B. Andreeva, Ogneupory No. 5, 224 (May 1965).

(14) R. A. Signorelli and T. W. Weeton, Aerospace Structural Materials, Conference Proccedings NASA SP-227.

(15) A. F. Mc Lean. The Application of Ceramics to the Small Gas Turbine, ASTM-706T-105.

(16) G. E. Hollox, Microstructure and Mechanical Behavior of Carbides, RIAS Report 68-10C, May 1968. Third Technical Report to ARO(D) DA-31-124-ARO-D-467. Seventh Technical Report to NASA NASw-1290